Mathematical Biosciences and Engineering

http://www.aimspress.com/journal/mbe

MBE, 20(6): 10304–10338.
DOI: 10.3934/mbe.2023452
Received: 20 October 2022
Revised: 02 December 2022
Accepted: 13 December 2022
Published: 31 March 2023

Research article

Data suggested hospitalization as critical indicator of the severity of the COVID-19 pandemic, even at its early stages

Stefanie Fuderer[1], Christina Kuttler[1], Michael Hoelscher[2,3,4], Ludwig Christian Hinske[5] and Noemi Castelletti[2,6,*]

[1] Department of Mathematics, Technical University of Munich, Garching, Germany

[2] Division of Infectious Diseases and Tropical Medicine, Medical Center of the University of Munich, Munich, Germany

[3] German Center for Infection Research (DZIF), partner site Munich, Munich, Germany

[4] Center for International Health (CIH), University Hospital, Munich, Germany

[5] Department of Anesthesiology, University Hospital, Munich, Germany

[6] Institute of Radiation Medicine, Helmholtz Zentrum München, Neuherberg, Germany

* **Correspondence:** Email: noemi.castellitti@med.uni-muenchen.de.

Abstract: COVID-19 has been spreading widely since January 2020, prompting the implementation of non-pharmaceutical interventions and vaccinations to prevent overwhelming the healthcare system. Our study models four waves of the epidemic in Munich over two years using a deterministic, biology-based mathematical model of SEIR type that incorporates both non-pharmaceutical interventions and vaccinations. We analyzed incidence and hospitalization data from Munich hospitals and used a two-step approach to fit the model parameters: first, we modeled incidence without hospitalization, and then we extended the model to include hospitalization compartments using the previous estimates as a starting point. For the first two waves, changes in key parameters, such as contact reduction and increasing vaccinations, were enough to represent the data. For wave three, the introduction of vaccination compartments was essential. In wave four, reducing contacts and increasing vaccinations were critical parameters for controlling infections. The importance of hospitalization data was highlighted, as it should have been included as a crucial parameter from the outset, along with incidence, to avoid miscommunication with the public. The emergence of milder variants like Omicron and a significant proportion of vaccinated people has made this fact even more evident.

Keywords: SARS-CoV-2; modeling; differential equation; hospitalization; prediction; data analysis

1. Introduction

In December 2019, some local health workers in Wuhan city (Hubei region, China) reported cases of pneumonia-like symptoms with an unknown cause. On February 11, 2020, the disease was officially named the coronavirus disease 2019 (COVID-19), and its cause was determined to be the severe acute respiratory syndrome coronavirus 2 (SARS-CoV-2) [1]. Following more than 118,000 confirmed COVID-19 cases in 114 countries and 4,291 deaths, the World Health Organization declared COVID-19 as a pandemic on March 11, 2020 [2]. Since then, there have been outbreaks worldwide with approximately 603 million confirmed cases and over 6.4 million deaths as of September 2022 [3].

The first cases of COVID-19 were detected in Germany's Munich municipality in late January 2020, and, due to the virus' high contagion rate, the number of cases rapidly increased [4]. To prevent the collapse of the healthcare system, the government quickly implemented non-pharmaceutical interventions, such as social distancing, face mask wearing, isolation of infected individuals, nationwide lockdowns and contact tracing, to slow down and control the virus' spread [1, 5]. In addition, vaccines against SARS-CoV-2 were promptly developed, and they have been available in Germany since December 26, 2020 [6]. All vaccines licensed in Germany have been observed to offer a high level of protection against severe cases of the disease [7].

Depending on the severity of symptoms, individuals infected with SARS-CoV-2 can be classified as follows [8]:

- mild,
- moderate (no or mild pneumonia, no or mild upper respiratory infection combined with febrile illness, dry cough and sore throat),
- severe with hospitalization (dyspnea, respiratory rate ≥ 30/min, blood oxygen saturation $\leq 93\%$ and/or pulmonary infiltrates $> 50\%$) and
- critical with hospitalization (respiratory insufficiency, septic shock due to bacterial superinfections, multiple organ dysfunction or failure, death).

In the first 20 weeks of the outbreak, the Robert Koch Institute (RKI) categorized about 80% of infections as mild or moderate, 18% as severe and the remaining 2% as critical [1, 8]. This resulted in a hospitalization rate of 20%. This value was significantly higher than the hospitalization rate of the flu in 2018–2019 (which was only 1.31%) and demonstrated the potential for a collapse of the healthcare system without intervention [9]. To manage the number of hospitalized cases, the daily number of new cases and the 7-day incidence became critical indicators [10]. However, the relationship between incidence and hospitalization changes depending on the virus variant, making it an unreliable indicator [10]. Due to this variability and the emergence of the Omicron variant, the focus has now shifted to the hospitalization rate [10].

Biology-based mathematical models can be used to contain the pandemic by predicting its spread. Linking such models with data is crucial for making informed decisions about public health, as evidenced by efforts to estimate the number of asymptomatic HIV infections and the impact of SARS and influenza outbreaks [11, 12]. With the ongoing COVID-19 pandemic, many researchers are fitting models to data to analyze the effects of government interventions such as contact restrictions, face mask usage and isolation of infected individuals. For instance, Chumachenko et al. [13] used machine

learning methods to predict COVID-19 incidence in multiple countries, while Ying and O'Clery [14] developed an agent-based model to study the spread of infection in a supermarket. Other researchers used relatively simple deterministic models composed of four or fewer compartments to analyze the spatial spread of COVID-19 [15–17], while Okuonghae and Omame [18] incorporated face mask usage and social distancing into their non-linear models of the SARS-CoV-2 epidemic in Nigeria. Barbarossa et al. [19] extended a deterministic model of SEIR type to simulate the effects of non-pharmaceutical interventions on the COVID-19 outbreak in Germany, and different strategies for mitigating the outbreak were explored.

In this study, we utilized a mathematical model of deterministic differential equations to simulate the spread of COVID-19 in Munich's population from January 2020 for over two years, encompassing four waves of the epidemic. Our approach focused on a biology-based method that mimicked the actual contribution of individuals in various compartments of an extended SEIR model, incorporating non-pharmaceutical interventions and, later, vaccinations. The transmission rates and reproduction number are proportional to the number of infectious contacts, which were reduced by the non-pharmaceutical measures. Our model is unique in that it captured the effects of these measures and quantified them not only between waves, but also within the same wave. Another distinctive aspect of our analysis is the inclusion of the number of patients in the intensive care unit (ICU) and normal hospital ward of Munich's hospitals. We fitted the model's parameters in a two-step process to prevent overfitting and increase stability in the model fitting. First, we fitted a model without hospitalization solely to the incidence data. Second, we extended the model with hospitalization compartments, using the parameters obtained from the first fit as given parameters to support the remaining hospitalization parameters' fit.

The emphasis in previous COVID-19 management strategies has been on tracking the number of cases, rather than focusing on the more critical issue of hospitalization. Our analysis shows that, from the outset of the pandemic, it was possible to simulate hospitalization data as a primary metric alongside case incidence. By doing so, we could have avoided confusion among the public and provided a clearer picture of the pandemic's status. This approach is especially important when dealing with milder variants like Omicron, in conjunction with a significant percentage of vaccinated individuals.

It is widely recognized that the number of infectious contacts is directly proportional to transmission rates and reproduction numbers. As a result, implementing non-pharmaceutical interventions reduces the number of contacts, which is reflected in Eqs (2.1) through (2.6) in the article. This quantification is a crucial aspect of our paper's development.

2. Materials and method

2.1. Prevalence data on daily detected COVID-19 cases

To gain an understanding of the pandemic situation, the daily number of COVID-19 infections can be used as one of multiple indicators. The RKI provides the 7-day incidence, which represents the number of new cases reported in the past 7 days per 100,000 inhabitants, and it is used to guide certain measures like the emergency brake [10]. The RKI platform offers the number of daily detected COVID-19 infections in Munich, starting from the first observed case on January 29, 2021. Figure 1 displays the occurrence of three main waves in Munich until the end of June, with varying (non-)

pharmaceutical interventions and hygiene awareness among the population influencing the pandemic's progression. Consequently, time-dependent model parameters were utilized not just for the three waves, but also for each wave individually (Table 1).

Table 1. Interventions during the first [20], second [21–23], third [24–26] and beginning of the fourth wave of COVID-19 in Munich. For each wave the first day is considered as day 0.

Intervention	**Time interval (date)**	**Time interval (days)**	**Contact rate**	**Transmission probability**	**Transmission rate**
First wave	2020/01/29–2020/06/15	day 0–138			
No interventions	2020/01/29–2020/03/21	day 0–52	c_0	p_0	β_0
Lockdown	2020/03/22–2020/04/19	day 53–81	$0.37c_0$	$0.3p_0$	$0.1 \cdot \beta_0$
Contact interventions	2020/04/20–2020/06/15	day 82–138	$0.5c_0$	$0.3p_0$	$0.15 \cdot \beta_0$
Second wave	2020/06/15–2021/02/15	day 138–383			
Contact interventions	2020/06/15–2020/11/01	day 0–139	$0.6c_0$	$p \cdot p_0$	$0.6 \cdot p\beta_0$
Lockdown light	2020/11/02–2020/12/15	day 140–183	$0.57c_0$	$p \cdot p_0$	$0.57p\beta_0$
Lockdown	2020/12/16–2021/01/18	day 184–217	c_3c_0	$p \cdot p_0$	$c_3p\beta_0$
FFP2 masks	2021/01/19–2020/02/15	day 218–245	c_4c_0	$p_4 \cdot p_0$	$c_4p_4\beta_0$
Third wave	2021/02/15–2021/06/30	day 383–518			
Lockdown	2021/02/15–2021/04/13	day 0–57	$0.35c_0$	$p \cdot p_0$	$0.35p\beta_0$
Emergency brake	2021/04/14–2021/05/10	day 58–84	c_2c_0	$p \cdot p_0$	$c_2p\beta_0$
Relaxations	2021/05/11–2021/06/06	day 85–111	c_3c_0	$p \cdot p_0$	$c_3p\beta_0$
Opening	2021/06/07–2021/06/30	day 112–135	$0.55c_0$	$p \cdot p_0$	$0.55p\beta_0$
Fourth wave	2021/06/30–2021/10/15	day 518–626			$\beta_0^{fourth} = 1.6\beta_0^{third}$
Relaxations	2021/06/30 – 2021/07/31	day 0–31	0.6	$p \cdot p_0$	$0.6p\beta_0^{fourth}$
More relaxations	2021/08/01–2021/09/30	day 32–92	c_2	$p \cdot p_0$	$c_2p\beta_0^{fourth}$
More relaxations	2021/10/01–2021/10/16	day 93–108	c_3	$p \cdot p_0$	$c_3p\beta_0^{fourth}$

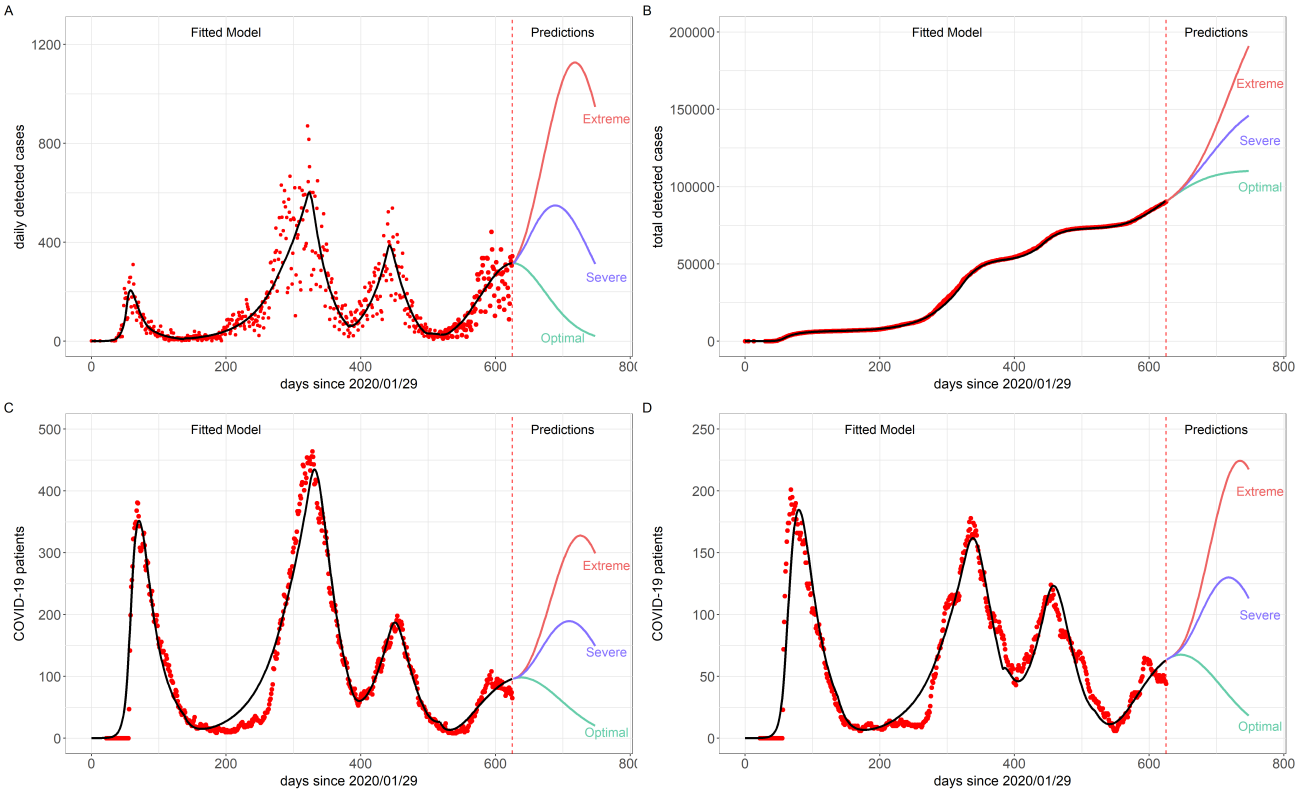

Figure 1. Data description and model results. Detected COVID-19 cases in Munich reported by the RKI [4]: (A) daily and (B) cumulative. Hospitalized COVID-19 cases in Munich for the normal ward (NW) stations (C) and ICUs (D). The solid black lines denote the results of the (A) and (B) preferred model and (C) and (D) hospitalization model. For the first and second waves, no vaccination compartments were needed.

2.1.1. First wave

In Munich, the first wave of COVID-19 occurred from late January to mid-June (refer to Figure 1). Three main interventions were implemented to prevent the spread of the disease:

1) no measures or, at least, no heavy measures were taken;

2) a lockdown was imposed throughout Munich;

3) the lockdown was lifted, but with severe contact reductions still in place (refer to Table 1).

To model the impact of these interventions, the time-dependent contact $c(t)$ and transmission probability $p(t)$ rates were utilized. During the lockdown period, a 63% reduction in contacts compared to normal was assumed, whereas the reduction during the lifting was around 50% [27]. Additionally, it was assumed that the population had greater awareness of hygiene, mask wearing, and social distancing during and after the lockdown, leading to an approximate 70% reduction in the transmission probability during contact [28]. This resulted in the following contact rate $c(t)$ and

transmission probability $p(t)$:

$$c(t) = \begin{cases} c_0 & \text{if } t \le 52 \\ 0.37c_0 & \text{if } 53 \le t \le 81 \\ 0.5c_0 & \text{if } 82 \le t \le 138 \end{cases}, \quad p(t) = \begin{cases} p_0 & \text{if } t \le 52 \\ 0.3p_0 & \text{if } 53 \le t \le 81 \\ 0.3p_0 & \text{if } 82 \le t \le 138, \end{cases} \tag{2.1}$$

where c_0 is the normal average contact rate and p_0 is the normal average transmission probability when no interventions are taken. With this it follows that the transmission rate $\beta(t) = c(t) \cdot p(t)$ is also time-dependent

$$\beta(t) = c(t)p(t) \approx \begin{cases} \beta_0 & \text{if } t \le 52, \\ 0.1\beta_0 & \text{if } 53 \le t \le 81, \\ 0.15\beta_0 & \text{if } 82 \le t \le 138, \end{cases} \tag{2.2}$$

where $\beta_0 = c_0 p_0$ is the normal average transmission rate without interventions.

2.1.2. Second wave

The time frame of the second wave of COVID-19 in Munich was from June 15th, 2020 to February 15th, 2021. Similar to the first wave, the second wave was split into distinct phases aligned with efforts to curb the spread of the disease (refer to Table 1). The initial intervention phase, spanning from June to October, resulted in a contact reduction of roughly 40%, while the subsequent "lockdown light" period saw a contact reduction of about 43% [27].

The contact reduction for the subsequent lockdown was also fitted. During the final intervention period, an FFP2 mask requirement was introduced in addition to the lockdown, which decreased the probability of transmission upon contact. The transmission probability only changed during the last intervention period and was also fitted. Therefore, the transmission rate for asymptomatic infected individuals is given by

$$\beta_a(t) \approx \begin{cases} 0.6p\beta_0 & \text{if } t \le 139, \\ 0.57p\beta_0 & \text{if } 140 \le t \le 183, \\ c_3 p\beta_0 & \text{if } 184 \le t \le 217, \\ c_4 p_4 \beta_0 & \text{if } 218 \le t \le 245, \end{cases} \tag{2.3}$$

where c_3 and c_4 are the fitted reductions of the transmission rate for the third and fourth intervention periods, respectively. In addition, the fitted reduction in transmission probability is described by p during the first three intervention periods, while p_4 describes the additional reduction of the transmission probability due to wearing the FFP2 masks. During the second wave, the test capacity increased and more infected individuals without symptoms were tested because of contact tracing.

2.1.3. Third wave

Between February 15, 2021 and June 30, 2021, Munich experienced its third wave of COVID-19 infections as shown in Figure 1. During this period, the lockdown measures from the previous wave remained in effect and were strengthened with an "emergency brake" beginning in mid-April. These

new measures included stricter contact reduction, a nighttime curfew and the closure of many stores, as summarized in Table 1 [24]. The contact reduction during the lockdown was assumed to be around 65%, while the contact rate during the "emergency brake" and relaxation period was fitted to the data. For the opening period, the contact rate was assumed to be similar to the beginning of the second wave. Consequently, the transmission rate is given by

$$\beta_a(t) \approx \begin{cases} 0.35p\beta_0 & \text{if } t \leq 57, \\ c_2 p\beta_0 & \text{if } 58 \leq t \leq 84, \\ c_3 p\beta_0 & \text{if } 85 \leq t \leq 111, \\ 0.55p\beta_0 & \text{if } 112 \leq t \leq 135. \end{cases} \tag{2.4}$$

New variants of the SARS-CoV-2 virus were detected in the first half of 2021, including the B.1.1.7 variant, also known as Alpha, which became the predominant strain in many countries during this time including Germany [29]. As of early March, the B.1.1.7 variant has accounted for over 40% of positive cases in Germany, with this proportion continuing to rise each week [30]. The B.1.1.7 variant is believed to have increased transmissibility, resulting in a higher transmission rate β_0 [31]. Meanwhile, in Germany, the vaccination campaign started in December 2020, and, by early June 2021, around 40% of Munich's population had received their first dose of the vaccine, while about 20% had received the second dose [32]. To ensure an adequate simulation of the third wave, this vaccination aspect is also taken into account in the model's structure.

2.1.4. Beginning of the fourth wave with further prediction

On June 30, 2021, Munich entered its fourth wave of the pandemic, despite various interventions and progress in vaccination having broken the third wave in spring of 2021. While 50% of Munich's population had received at least one vaccine dose and 36% had been fully vaccinated by the end of June 2021, the number of cases rose again. The Delta variant of SARS-CoV-2, which is approximately 60% more transmissible than the Alpha variant, became increasingly prevalent in Germany during the end of the third wave and the beginning of the fourth wave. By mid-July 2021, the Delta variant accounted for 74% of all cases in Germany [30]. To estimate the transmission rate during the fourth wave, the fitted transmission rate during the third wave for the Alpha variant (β_0) was used as a baseline, as it was the dominant strain at the time:

$$\beta_0^{fourth} = 1.6 \cdot \beta_0^{third}. \tag{2.5}$$

During July 2021, there were additional measures taken to ease COVID-19 restrictions, including increased capacity at outdoor and cultural events, extended hours for restaurants, relaxed mask rules and the reopening of bar interiors, as shown in Table 1 [33–35]. Contact reduction during July 2021 was assumed to be similar to that of the previous summer. For the intervention period from August to September 2021, the contact reduction was estimated. In October 2021, further relaxations were implemented, such as the reopening of clubs in Munich [36]. The contact reduction for October was

also estimated. These measures resulted in an average transmission rate for asymptomatic individuals:

$$\beta_a^{fourth}(t) = \begin{cases} 0.6p\beta_0^{fourth} & \text{if } 0 \le t \le 31, \\ c_2 p\beta_0^{fourth} & \text{if } 32 \le t \le 93, \\ c_3 p\beta_0^{fourth} & \text{if } 94 \le t \le 109. \end{cases} \tag{2.6}$$

According to [33], it has been demonstrated that all vaccines authorized in Germany provide lower protection against the Delta variant, especially in individuals who have only received one dose. As a result, a vaccine ineffectiveness factor σ has been introduced, which depends on the time elapsed since the first dose. The fourth wave was considered to be dominated by the Delta variant approximately one week after it began; σ is hence defined by

$$\sigma(t) = \begin{cases} \sigma_{alpha} & \text{if } 0 \le t \le 7, \\ \sigma_{delta} & \text{if } 8 \le t, \end{cases} \tag{2.7}$$

where $\sigma_{alpha} = 0.25$ is the vaccine inefficacy after the first dose against infection with the Alpha variant and σ_{delta} is the fitted vaccine inefficacy after the first dose against infection with the Delta variant.

The parameters for predicting the number of new COVID-19 cases were fitted by using data from the first few months of the fourth wave, up until October 15, 2021. To make predictions for future periods, various scenarios were considered. These include an optimal scenario, where vaccination rates and contact rates remain constant from October 15, 2021, a severe scenario where vaccination rates decrease while contact rates increase and an extreme scenario where vaccination is completely stopped and contact rates increase rapidly.

2.2. Number of COVID-19 hospitalized patients: IVENA software

The crucial indicators for determining the severity of the pandemic are the number of hospitalized patients and those requiring intensive care (IC), as stated in [10]. Maintaining control over these numbers is essential in making decisions regarding potential interventions.

A web-based software called Interdisciplinary Evidence of Care (IVENA) is utilized to facilitate the exchange of information among emergency departments, ambulance services and clinics. This tool aids in optimizing the allocation of resources and patient management, and it also reports on the number of COVID-19 patients in normal wards and ICUs across Munich hospitals, as cited in [37].

However, in the IVENA dataset, some days in October and November 2021 were missing data on the number of patients in normal wards or ICUs in Munich hospitals. To fill these gaps, alternative data sources were used, as referenced in [32].

2.3. Biology-based deterministic models: Considering different types of infectious individuals

The analysis uses models based on the SEIR theory, which assumes that susceptible individuals (S) can become infected through contact with infected individuals (I) [12]. After infection, individuals move from the susceptible class to the exposed class (E), where they are asymptomatic and not infectious. Infected individuals then move to the infectious class (I) and eventually recover (R) [38]. A more detailed description of the SEIR model is available in the Supplemental Material.

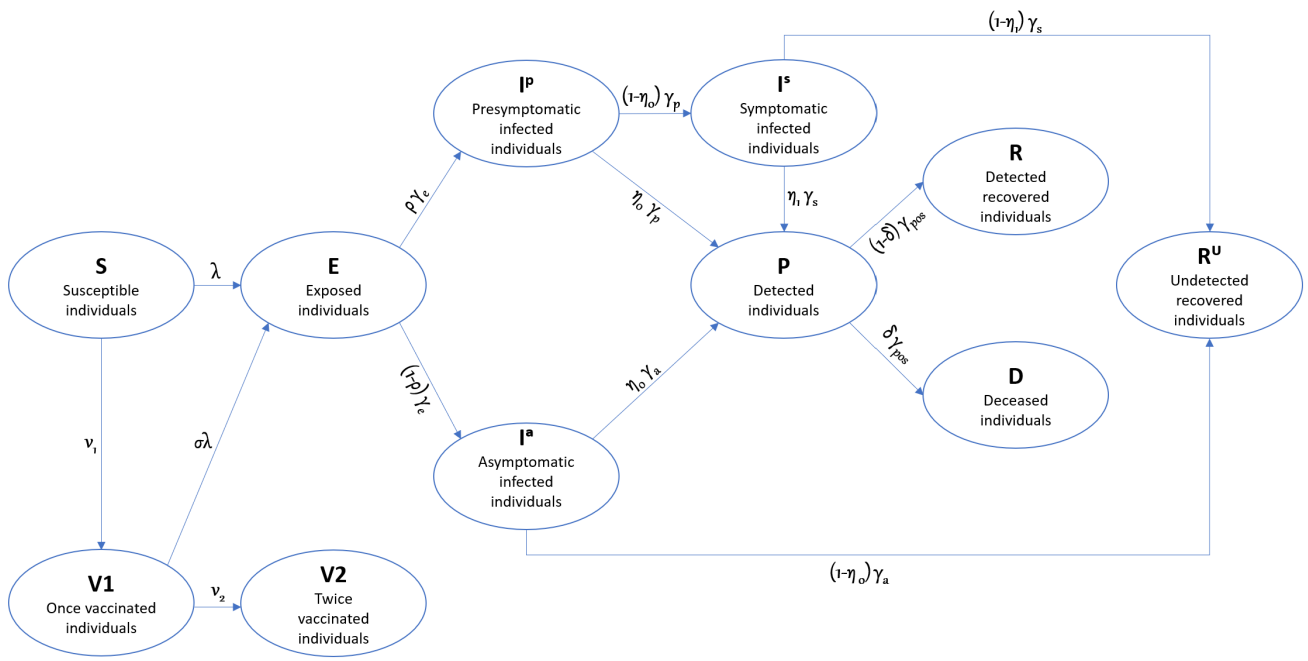

(a)

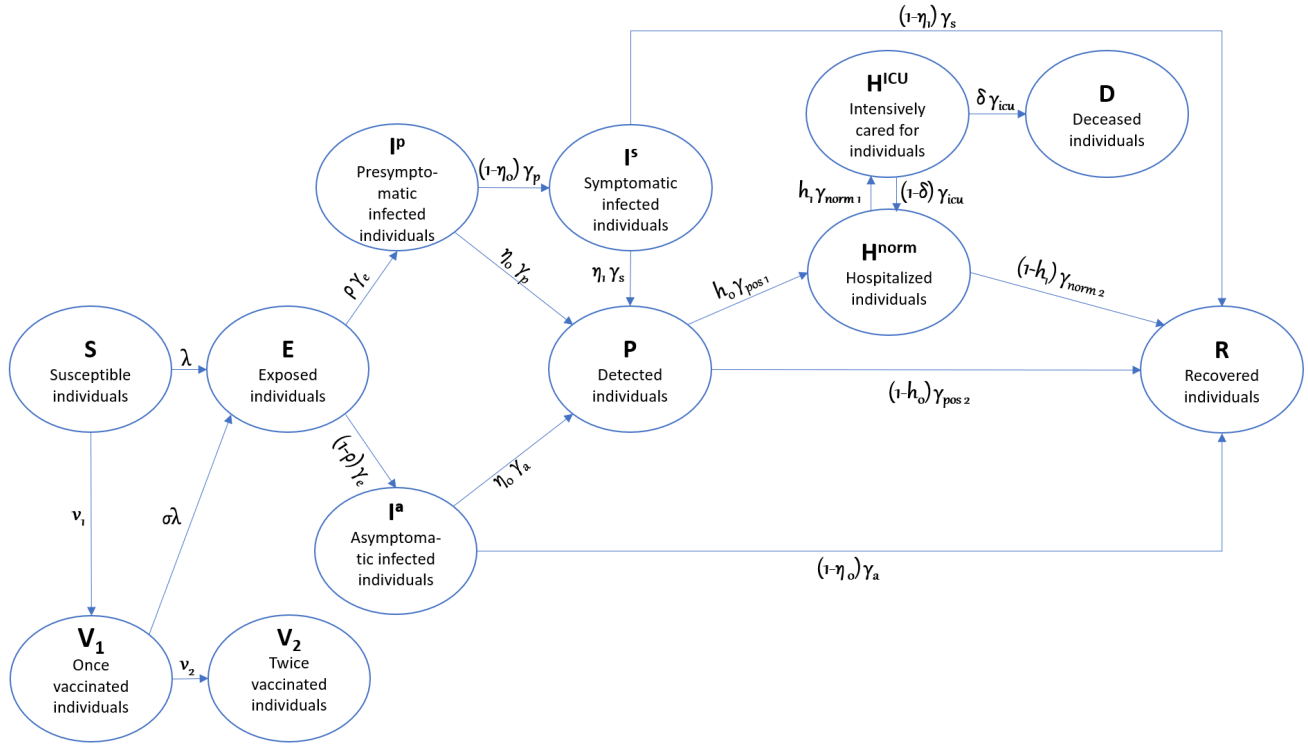

(b)

Figure 2. Schematic description of the applied models: (A) the preferred model and (B) the hospitalization model, both with vaccination expansion.

The top of Figure 2 is an extension of the SEIR model, with the infectious class (I) split into asymptomatic infected individuals (I^a), presymptomatic infected individuals (I^p), symptomatic infected individuals (I^s) and detected individuals (P). After infection, individuals move to the exposed class E, where they are asymptomatic and not infectious. Exposed individuals can hence develop symptoms with rate ρ, moving first to the presymptomatic class I^p, then to the symptomatic class I^s and finally to the detected class P with rate η_1. Exposed people staying asymptomatic (probability $1 - \rho$) move directly to the detected class (P) with rate η_0. Individuals in the asymptomatic, presymptomatic, symptomatic and detected classes spend an average time of $\frac{1}{\gamma_a}$, $\frac{1}{\gamma_p}$, $\frac{1}{\gamma_s}$ and $\frac{1}{\gamma_{pos}}$, respectively, before recovering (R from detected and R^u for undetected cases) and becoming immune to reinfection. Individuals who die (D) from COVID-19 are removed from the population. In Germany, it is very likely that a critical infection will be detected. Therefore, we assume that infected individuals who have not been diagnosed with COVID-19 are unlikely to die due to the disease. The case fatality ratio (CFR) of detected infections δ was calculated with the help of the RKI data [4]. The transmission rates for asymptomatic, presymptomatic, symptomatic and detected individuals are β_a, β_p, β_s and β_{pos}, respectively. We assume that asymptomatic and presymptomatic infected individuals do not restrict their contacts to others and therefore have higher transmission rates than symptomatic and detected infective people. Vaccination is assumed to be given only to susceptible individuals (S) at a rate of v_1, who then move to compartment V_1. After the first dose, individuals have approximately 75% protection against infection with SARS-CoV-2, as defined by $(1 - \sigma)$ [39]. After the second dose, individuals move to compartment V_2 at a rate of v_2. Fully vaccinated individuals are assumed to be protected against infection, and the time lag of two weeks after the second dose needed to build up immunity is neglected for simplicity.

The preferred model is presented in Figure 2 (top), and it is described by the following system of differential equations:

$$\begin{aligned}
\dot{S} &= -\lambda S - v_1 S, \\
\dot{E} &= \lambda S + \sigma\lambda V_1 - \gamma_e E, \\
\dot{V}_1 &= v_1 S - \sigma\lambda V_1 - v_2 V_1, \\
\dot{V}_2 &= v_2 V_1, \\
\dot{I}^a &= (1-\rho)\gamma_e E - \gamma_a I^a, \\
\dot{I}^p &= \rho\gamma_e E - \gamma_p I^p, \\
\dot{I}^s &= (1-\eta_0)\gamma_p I^p - \gamma_s I^s, \\
\dot{P} &= \eta_0\gamma_a I^a + \eta_0\gamma_p I^p + \eta_1\gamma_s I^s - \gamma_{pos} P, \\
\dot{R} &= (1-\delta)\gamma_{pos} P, \\
\dot{D} &= \delta\gamma_{pos} P, \\
\dot{R}^u &= (1-\eta_1)\gamma_s I^s + (1-\eta_0)\gamma_a I^a,
\end{aligned} \tag{2.8}$$

where $\lambda(t) = \frac{\beta_a I^a + \beta_p I^p + \beta_s I^s + \beta_{pos} P}{N-D}$ is the force of infection and N the total population size. For this model we assume that the transmission rate of asymptomatic infectious individuals β_a is time-dependent (see Chapters 2.1.1–2.1.4). Consequently, it follows that the other transmission rates, β_p, β_s and β_{pos}, are also time-dependent. To model the epidemic already since the first days cases were tested, as initial values for the preferred model, we used $S(0) = N - 2$, $E(0) = V_1(0) = V_2(0) = I^a(0) = I^p(0) = R(0) = D(0) = R^u(0) = 0$ and $I^s(0) = P(0) = 1$. The whole population is susceptible, except for two people: one is a detected individual and the other a symptomatic detected individual. All other compartments are empty. For waves 1 and 2, the initial conditions for the vaccination compartments were $V_1(0) = V_2(0) = 0$ (no vaccination available, so compartments are empty), while for wave 4, $V_1(0) = 25000$ and $V_2(0) = 15000$ (vaccination campaign started fully working). For time intervals without a vaccination campaign, we set the rate $v_1 = 0$, keeping the compartment empty until the start of vaccination. To compare the model results with the RKI data, the newly detected infections $\hat{d}(t)$ at day t need to be defined. At the starting point, the number of daily detected cases corresponds to the number of detected individuals at day 0: $P(0)$. For any further time point $t > 0$, our approach was as follows:

- The population N is constant, including deaths D if included in the model: $N(t) - N(t+1) = 0$;
- The newly detected cases on day t, $\hat{d}(t)$, correspond only to the individuals who leave compartment S at that day, $S(t)$ and not of interest are all other "internal changes" between different compartments. To calculate this in formula, it is the individuals in S on that day t, $S(t)$, minus the individuals in S the next day, $S(t+1)$: $S(t) - S(t+1) = \hat{d}(t)$;
- In an extended SIR-model, the individuals leaving S can go to more compartments than only I. In our specific case, they can go to the compartments of detected individuals (P), to dead individuals (D) and to recovered individuals (R). Therefore, for out model, the total population corresponds to $N = S + P + D + R$, or $S = N - P - D - R$;
- Looking at individuals leaving compartment S, this can be formulated as follows: $\hat{d}(t) = S(t) - S(t+1) = N(t) - N(t+1) - P(t) + P(t+1) - D(t) + D(t+1) - R(t) + R(t+1)$;
- Remembering that we assume a constant population N(t)-N(t+1) = 0, this leads to $\hat{d}(t) = S(t) - S(t+1) = P(t+1) - P(t) + D(t+1) - D(t) + R(t+1) - R(t)$.

The formula can be interpreted as follows: the daily detected cases in the RKI data can be located to different compartments in the model. They can be just "detected individuals" by polymerase chain reaction (PCR) or later on by rapid testing. They could be detected after death, which really happened in the first two waves since the laboratories were struggling with test capacities. Or, they could be detected at recovery. The daily detected cases $\hat{d}(t)$ at day t are hence calculated by the following formula:

$$\hat{d}(t) = \begin{cases} P(0) & \text{if } t = 0, \\ [P(t+1) - P(t)] + [D(t+1) - D(t)] + [R(t+1) - R(t)] & \text{if } t > 0. \end{cases}$$

Parameter assumptions are given in Tables 2 and 3.

Table 2. Parameters of the preferred model for wave one and two without hospitalization compartments. Short forms: CFR, mean duration (MD).

Parameter	Description	Value (unit) [Refs.]
First wave		
β_0	Init. transm. rate of asympt. I	0.66 $\frac{1}{d \cdot \text{individual}}$ [fitted]
β_p	Transm. rate of presympt. I	β_a [assumed]
β_s	Transm. rate of symptomatic I	$0.6\beta_a$ [assumed]
β_{pos}	Transm. rate of detected I	$0.1\beta_a$ [assumed]
$\frac{1}{\gamma_e}$	Mean latent period	5.5 d [38, 40]
$\frac{1}{\gamma_a}$	MD of asympt. infection	6 d [assumed]
$\frac{1}{\gamma_p}$	MD of presympt. infection	2 d [38]
$\frac{1}{\gamma_s}$	MD of sympt. infection	7 d [assumed]
$\frac{1}{\gamma_{pos}}$	MD of infection	6 d [fitted]
ρ	Prob. of developing symptoms	0.69 [41]
η_0	Prob. of detection while asympt.	0.07 [assumed]
η_1	Prob. of detection while sympt.	0.56 [fitted]
δ	CFR of detected infections	0.033 [4]
v_1	Vacc. rate first dose	0
v_2	Vacc. rate second dose	0
N	Tot. population size	1,484 million [42]
Second wave (new parameters)		
$p\beta_0$	Init. transm. rate of asympt. I with reduction in transm. prob.	0.37 $\frac{1}{d \cdot \text{individual}}$ [fitted]
c_3	Reduction in contact rate (third intervention period)	0.27 [fitted]
$c_4 p_4$	Reduction in transm. rate (fourth intervention period)	0.24 [fitted]
η_0	Prob. of detection while asympt.	0.15 [assumed]
η_1	Prob. of detection while sympt.	0.85 [assumed]
δ	CFR of detected infections	0.019 [4]

Table 3. Parameters of the preferred model for waves three and four with vaccination compartments. Short forms: CFR.

Parameter	Description	Value (unit) [Refs.]
Third wave (new parameters)		
$p\beta_0$	Init. transm. rate of asympt. I with reduction in transm. prob.	0.79 $\frac{1}{d\cdot\text{individual}}$ [fitted]
c_2	Reduction in contact rate (second intervention period)	0.11 [fitted]
c_3	Reduction in transm. rate (third intervention period)	0.11 [fitted]
η_0	Prob. of detection while asympt.	0.25 [assumed]
η_1	Prob. of detection while sympt.	0.9 [assumed]
δ	CFR of detected infections	0.008 [4]
N	Tot. population size	1,488 million [42]
Third wave with vaccination		
$p\beta_0$	Init. transm. rate of asympt. I with reduction in transm. prob.	0.82 $\frac{1}{d\cdot\text{individual}}$ [fitted]
c_2	Reduction in contact rate	0.15 [fitted]
c_3	Reduction in transm. rate	0.15 [fitted]
v_1	Vacc. rate first dose, $t \leq 75$	$0.0014\frac{1}{d\cdot\text{individual}}$ [fitted]
	Vacc. rate first dose, $75 \leq t \leq 135$	$0.0243\frac{1}{d\cdot\text{individual}}$ [fitted]
v_2	Vacc. rate second dose, $t \leq 60$	$0.0325\frac{1}{d\cdot\text{individual}}$ [fitted]
	Vacc. rate second dose, $60 \leq t \leq 135$	$0.0151\frac{1}{d\cdot\text{individual}}$ [fitted]
σ	Vacc. inefficacy after first dose	0.25 [39]
Fourth wave with vaccination		
c_2	Reduction in contact rate	0.65 [fitted]
c_3	Reduction in transm. rate	0.66 [fitted]
δ	CFR of detected infections	0.004 [4]
σ_{alpha}	Vacc. inefficacy after first dose against Alpha-variant infection	0.25 [39]
σ_{delta}	Vacc. inefficacy after first dose	0.6 [fitted]
v_1	Vacc. rate first dose, $t \leq 75$	$0.0101\frac{1}{d\cdot\text{individual}}$ [fitted]
	Vacc. rate first dose, $75 \leq t \leq 108$	$0.0171\frac{1}{d\cdot\text{individual}}$ [fitted]
v_2	Vacc. rate second dose, $t \leq 50$ against Delta-variant infection	$0.0129\frac{1}{d\cdot\text{individual}}$ [fitted]
v_2	Vacc. rate second dose, $50 \leq t \leq 108$ against Delta-variant infection	$0.0037\frac{1}{d\cdot\text{individual}}$ [fitted]

2.4. Model expansion with hospital compartments

In order to simulate the number of COVID-19 patients in both regular hospital wards and ICUs in Munich, the model must be expanded. When a person is diagnosed with the virus and has mild or no symptoms, they stay in compartment P. If a person's symptoms are severe, they are admitted to the regular hospital ward (H^{norm}), with the probability of hospitalization described as h_0. Those in the hospital who develop critical symptoms have a probability of h_1 of being transferred to the ICU (H^{ICU}). Patients in the ICU who do not survive the virus (death rate δ) are moved to the deceased compartment (D). Once a patient's condition stabilizes in the ICU, they are transferred back to the regular ward for continued monitoring, but no longer require IC. Finally, after their infection has resolved, all individuals move to the recovered compartment (R). The hospitalization model's dynamics are displayed at the bottom of Figure 2. Additionally, more information regarding parameter assumptions can be found in Tables 4 and 5. The hospitalization model is then given by the following system of differential equations:

$$\begin{aligned}
\dot{S} &= -\lambda S - v_1 S,\\
\dot{E} &= \lambda S + \sigma\lambda V_1 - \gamma_e E,\\
\dot{V}_1 &= v_1 S - \sigma\lambda V_1 - v_2 V_1,\\
\dot{V}_2 &= v_2 V_1,\\
\dot{I}^a &= (1-\rho)\gamma_e E - \gamma_a I^a,\\
\dot{I}^p &= \rho\gamma_e E - \gamma_p I^p,\\
\dot{I}^s &= (1-\eta_0)\gamma_p I^p - \gamma_s I^s,\\
\dot{P} &= \eta_0\gamma_a I^a + \eta_0\gamma_p I^p + \eta_1\gamma_s I^s - (h_0\gamma_{pos_1} + (1-h_0)\gamma_{pos_2})P,\\
\dot{H}^{norm} &= h_0\gamma_{pos_1} P + (1-\delta)\gamma_{icu} H^{ICU} - (h_1\gamma_{norm_1} + (1-h_1)\gamma_{norm_2})H^{norm},\\
\dot{H}^{ICU} &= h_1\gamma_{norm_1} H^{norm} - \gamma_{icu} H^{ICU},\\
\dot{D} &= \delta\gamma_{icu} H^{ICU},\\
\dot{R} &= (1-\eta_0)\gamma_a I^a + (1-\eta_1)\gamma_s I^s + (1-h_0)\gamma_{pos_2} P + (1-h_1)\gamma_{norm_2} H^{norm},
\end{aligned} \tag{2.9}$$

where $\lambda(t) = \frac{\beta_a I^a + \beta_p I^p + \beta_s I^s + \beta_{pos} P}{N-D}$ is the force of infection and N is the total population size. $\beta_a(t)$ is time-dependent and defined in Chapters 2.1.1–2.1.4.

Table 4. Parameters of the preferred model with hospitalization for waves one and two. Short forms: CFR, MD, mean time (MT), NW, ICU, IC.

Parameter	Description	Value (unit) [Refs.]
First wave		
$\frac{1}{\gamma_{pos_1}}$	MD from detection to hospitalization	2 d [fitted]
$\frac{1}{\gamma_{pos_2}}$	MD of infection	8 d [fitted]
$\frac{1}{\gamma_{norm_1}}$	MT from hospitalization to ICU	1 d [38]
$\frac{1}{\gamma_{norm_2}}$	MT on NW, no IC	7 d [38]
$\frac{1}{\gamma_{icu}}$	MT on ICU	9 d [8]
h_0	Prob. of hospitalization	0.14 [fitted]
h_1	Prob. of requiring IC	0.07 [fitted]
δ	CFR of detected infections	0.34 [43]
ρ	Prob. of developing symptoms	0.69 [41]
η_0	Prob. of detection while asympt.	0.07 [assumed]
v_1	Vacc. rate first dose	$0\ \frac{1}{d\cdot\text{individual}}$
v_2	Vacc. rate second dose	$0\ \frac{1}{d\cdot\text{individual}}$
Second wave		
$\frac{1}{\gamma_{pos_1}}$	MD from detection to hospitalization	2 d [fitted]
$\frac{1}{\gamma_{pos_2}}$	MD of infection	6 [fitted]
h_0	Prob. of hospitalization	0.06 [fitted]
h_1	Prob. of requiring IC	0.04 [fitted]
η_0	Prob. of detection while asympt.	0.15 [assumed]
η_1	Prob. of detection while sympt.	0.85 [assumed]

2.5. Data fitting

In order to accurately represent the data, a two-step method was employed. Initially, a model excluding hospitalization was used to fit the incidence data for all rounds. Subsequently, the model was expanded to incorporate hospitalization compartments, and the parameters from the first fit were utilized as fixed parameters to achieve a proper fit for the remaining hospitalization parameters. This approach prevents overfitting and enhances the stability of the fit, resulting in a final model that accurately fits the hospitalization data. The advantage of this technique is its ability to merge two distinct datasets. The incidence model provides information on pandemic progression, whereas the second step focuses on hospitalization. Since the pandemic's development is identical with or without hospitalization parameters, the parameters obtained in the first fit can be directly integrated into the second model for a better fit.

Table 5. Parameters of the preferred model with hospitalization. Short forms: MD and IC.

Parameter	Description	Value (unit) [Refs.]
Third wave		
$\frac{1}{\gamma_{pos_1}}$	MD from detection to hospitalization	2 d [fitted]
$\frac{1}{\gamma_{pos_2}}$	MD of infection	6 d [fitted]
h_0	Prob. of hospitalization	0.06 [fitted]
h_1	Prob. of requiring IC	0.08 [fitted]
η_0	Prob. of detection while asympt.	0.25 [assumed]
η_1	Prob. of detection while sympt.	0.90 [assumed]
ν_1	Vacc. rate first dose, $t \leq 75$	$0.004 \frac{1}{d \cdot \text{individual}}$ [fitted]
	Vacc. rate first dose, $75 \leq t \leq 135$	$0.008 \frac{1}{d \cdot \text{individual}}$ [fitted]
ν_2	Vacc. rate second dose, $t \leq 60$	$0.03 \frac{1}{d \cdot \text{individual}}$ [fitted]
	Vacc. rate second dose, $60 \leq t \leq 135$	$0.024 \frac{1}{d \cdot \text{individual}}$ [fitted]
σ	Vacc. inefficacy after first dose	0.25 [39]
Fourth wave		
h_0	Prob. of hospitalization	0.014 [fitted]
h_1	Prob. of requiring IC	0.077 [fitted]
ν_1	Vacc. rate first dose, $t \leq 75$	$0.0464 \frac{1}{d \cdot \text{individual}}$ [fitted]
	Vacc. rate first dose, $75 \leq t \leq 108$	$0.04 \frac{1}{d \cdot \text{individual}}$ [fitted]
ν_2	Vacc. rate second dose, $t \leq 50$	$0.0085 \frac{1}{d \cdot \text{individual}}$ [fitted]
	Vacc. rate second dose, $50 \leq t \leq 108$	$0.0012 \frac{1}{d \cdot \text{individual}}$ [fitted]

2.6. Positivity and boundedness

To be realistic and meaningful, solutions of our model system should preserve positivity, or, to be more precise non-negativity and boundedness. As is usual in this context, all parameter values are assumed to be non-negative. One can easily see that a solution of (2.9) with non-negative initial values at $t = 0$ for all variables stays non-negative for all $t \geq 0$. For the variables V_2, D and R, this holds in general, as there are only non-negative entries on the corresponding right-hand sides; for all other variables, the derivative is also ≥ 0 if the corresponding variable itself is equal to zero, using that $0 \leq \rho, \eta_0, \eta_1, h_0, h_1 \leq 1$ by definition.

For the boundedness, let us consider the sum of all variables, which corresponds to the total population in the system. Its time derivative satisfies

$$\dot{S} + \dot{E} + \dot{V}_1 + \dot{V}_2 + \dot{I}^a + \dot{I}^p + \dot{I}^s + \dot{P} + \dot{H}^{norm} + \dot{H}^{ICU} + \dot{D} + \dot{R} = 0,$$

as all terms on the right-hand side of (2.9) cancel out. Thus, the total population stays constant, and it is a closed compartmental model. As we have seen already that all variables stay non-negative, it follows directly that all variables are bounded by the sum of the initial values: $S(0) + E(0) + V_1(0) + V_2(0) + I^a(0) + I^p(0) + I^s(0) + P(0) + H^{norm}(0) + H^{ICU}(0) + D(0) + R(0)$.

Please note that this can be shown analogously for the other model variants here.

2.7. Parameter estimation

To obtain the best estimated parameter set $\theta = (p_1, ..., p_k)$ that is dependent on unknown parameters $p_1, ..., p_k$, and to analyze the performance of a model, the model itself has to be validated using real-life data [44]. In this analysis, we first model the prevalence that directly corresponds to the model-output $I(t)$. Following, the fitted parameters are used to support a further fit with the hospitalization data that directly correspond to the model outputs H^{norm} and H^{ICU}.

To find the best estimated parameter set θ, we determine the sum-of-squares error (SSE), i.e., the sum of squares of the vertical distances from the real data points $d(t)$ to the points of the solution curve $I(t)$ of the model [44]:

$$SSE = \sum_t (d(t) - I(t))^2. \tag{2.10}$$

To achieve the optimal performance of the model, the least-squares approach is hence applied, minimizing the SSE [44]:

$$\hat{\theta} = \underset{\theta}{\operatorname{argmin}}\, SSE(\theta). \tag{2.11}$$

The programming language R, version 4.0.5, was used for model fitting. Furthermore, for minimizing, the SSE the *L-BFGS-B* optimization method was used. A definition of the goodness-of-fit method, Akaike information criterion (AIC) and model comparison are presented in detail in the Supplemental Material.

3. Results

3.1. Modeling the number of daily detected and hospitalized COVID-19 cases

The model results for the first wave are presented in Figure 3(A) and (B) and Tables 2 and 4. It can be appreciated that the model adequately simulates the real data. The results obtained for the last day of the first wave will be used as initial values for modeling the second wave, the results of which are presented in Figure 3(C) and (D). Also, for the second wave, it can be seen that the model captures the structure of the data, confirming the fact that neither the virus nor the immune status of the population changed from the first to the second wave. The parameters used for the third wave are summarized in Tables 3 and 5. The results of the last day of the second wave were used as initial values. Results of the third wave can be seen in Figure 3(E) and (F). Although a lockdown was implemented, the number of COVID-19 cases increased again, and the third wave began. As new variants appeared, the model needed to be adapted, and the parameters were changed accordingly. Toward the end of the third wave, there was a discrepancy between the modeled number of daily detected COVID-19 cases and those reported by the RKI, which was solved by adding compartments representing the vaccinated population [32]. The parameters used for this model are presented in Tables 3 and 5, and the results are shown in Figure 4. The accuracy of the model was significantly improved by incorporating the vaccinated population.

Model results of the hospitalizations in Munich are presented in Figure 5 and Tables 4 and 5. It can be noticed that, for all three waves, the structure of the data can be well captured by the model. Due to its importance in the third wave, the model with vaccination compartments was directly applied due to its effectiveness.

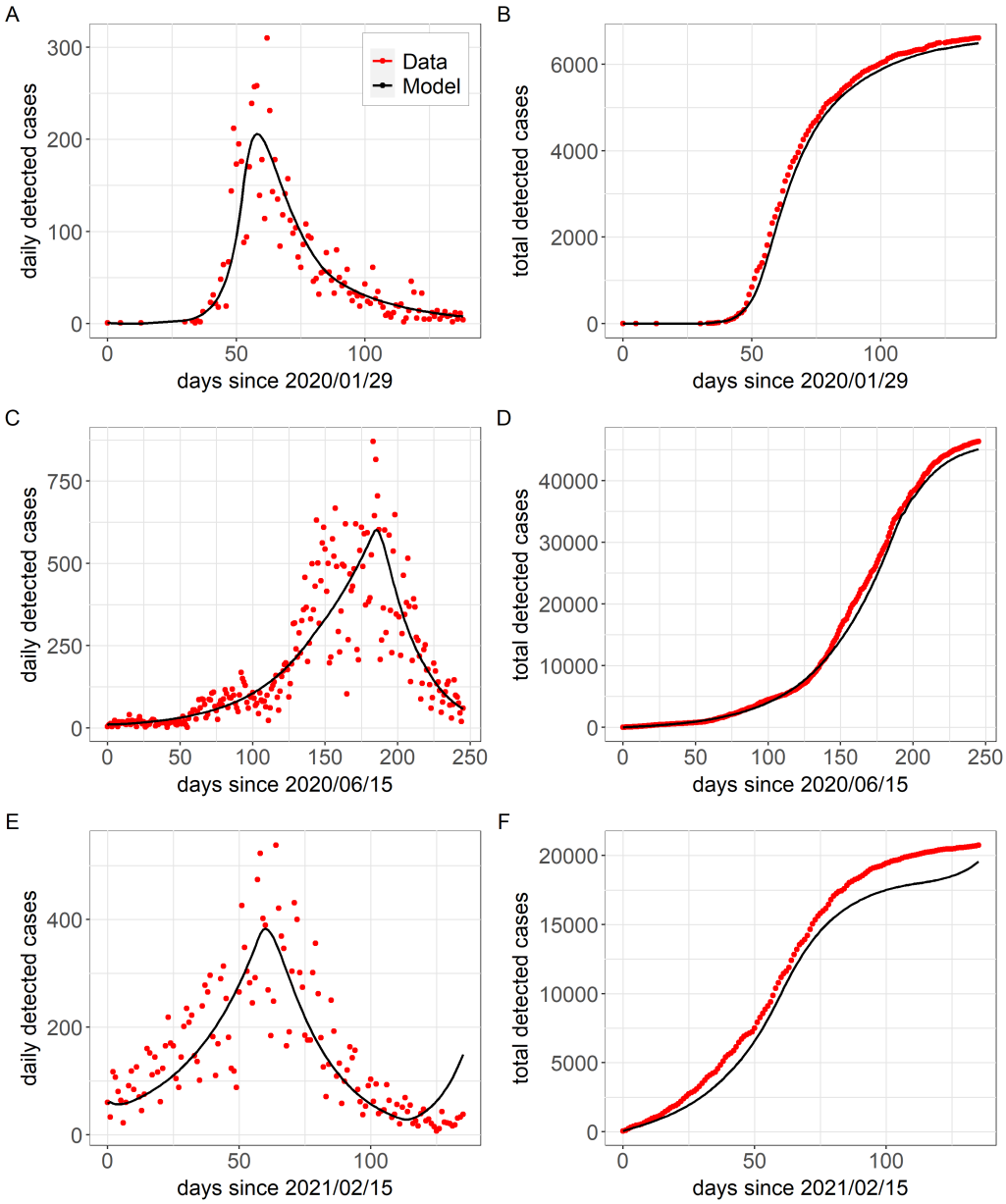

Figure 3. Performance evaluation of the preferred model: Comparison of model output (black) with RKI data (red). (A), (C) and (D): Daily detected COVID-19 cases in Munich in waves one, two and three, respectively. (B), (D) and (E): Total detected COVID-19 cases in Munich in waves one, two and three, respectively. The preferred model captures the structure of the data for the first and second wave very well. For the third wave some discrepancies can be noticed.

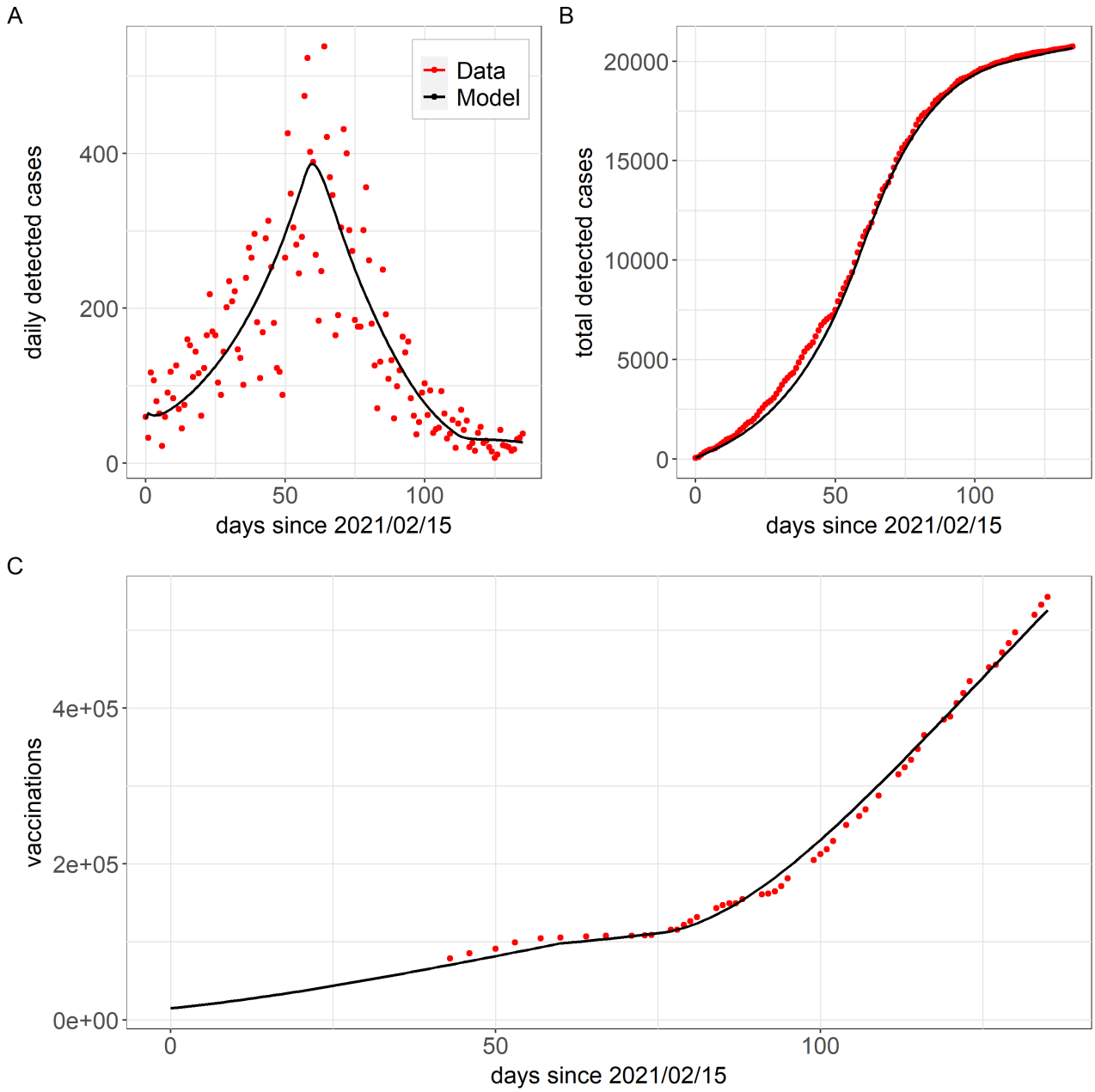

Figure 4. Performance evaluation of the preferred model with vaccination extension for wave three: Comparison of model output (black) with RKI data (red). (A): Daily detected COVID-19 cases in Munich. (B): Total detected COVID-19 cases in Munich. (C): Completely vaccinated individuals in Munich, reported by [32].

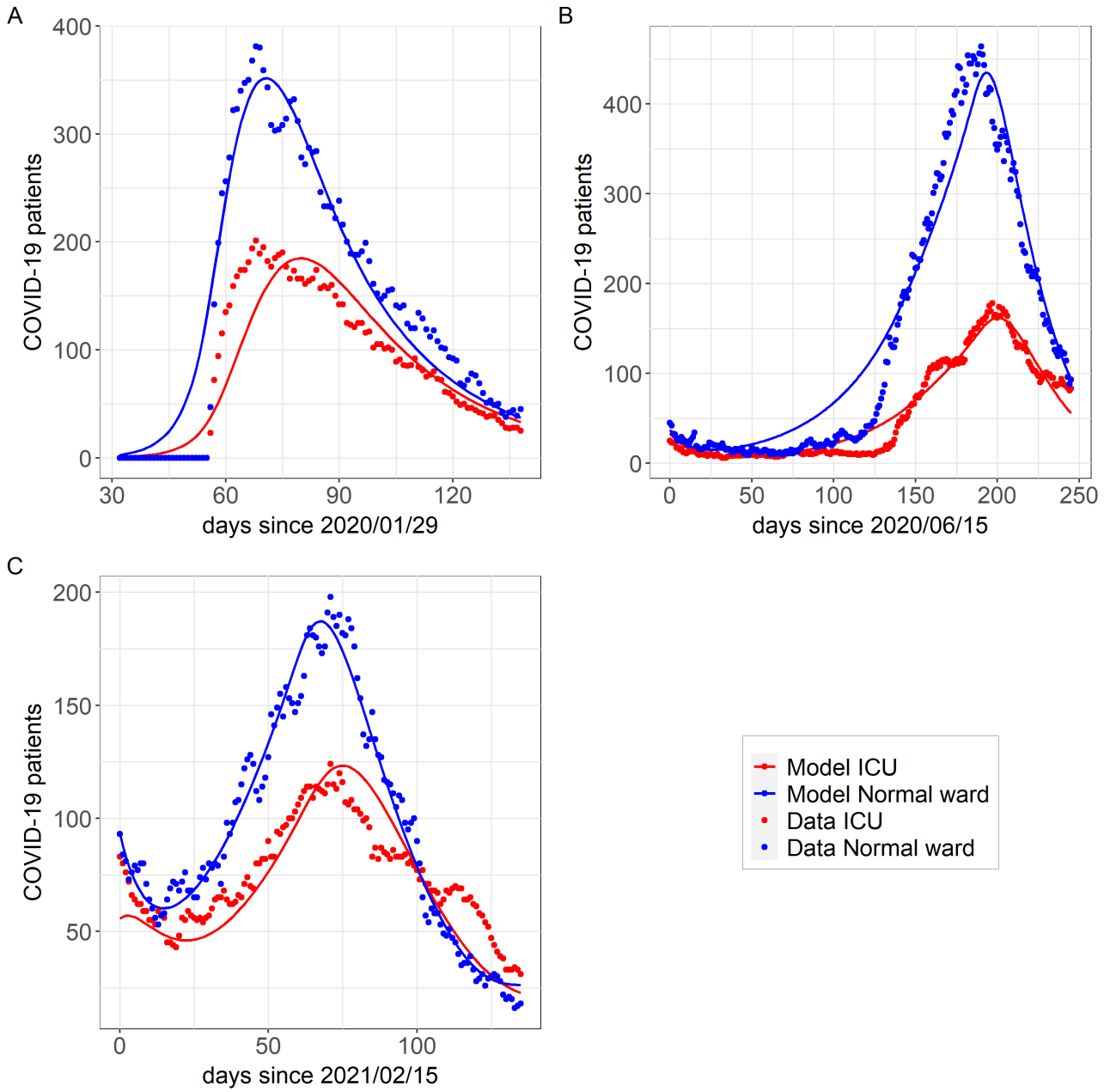

Figure 5. Performance evaluation of the hospitalization model: Comparison of model output (lines) with IVENA data (dots) for (A) the first wave, (B) the second wave and (C) the third wave. The NW station is represented in blue, while the ICU is represented in red. For wave one and two, no vaccination compartments were needed.

3.2. Predictions for the fourth wave

The beginning of the fourth wave was used as the starting point for predictions. From Figure 6, it can be seen that the amount of new COVID-19 cases and, therefore, also the number of hospitalized

patients, dramatically depends on the vaccination campaign. It can be appreciated that the time of the peak shifts with that dependency. The lower the vaccination success, the higher and later the peak.

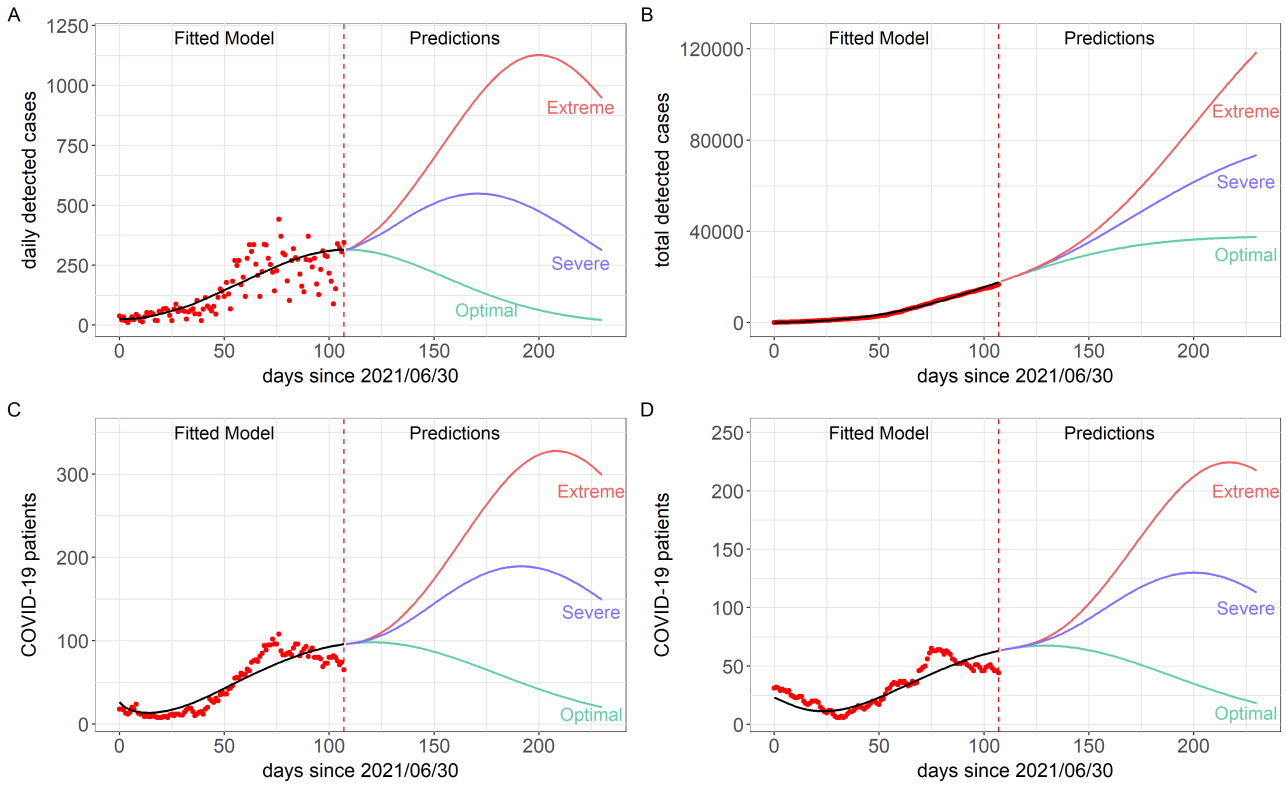

Figure 6. Model predictions for wave four: Optimal scenario (green), severe scenario (blue) and extreme scenario (violet). Model prediction for daily (A) and cumulative (B) detected COVID-19 cases in Munich. Model prediction for hospitalized COVID-19 patients in the ward station (C) and ICU (D).

4. Conclusions

We utilized biology-based mathematical models to simulate the number of new COVID-19 infections and hospitalizations in Munich's ward and ICUs during the first four waves of the pandemic. Our findings suggest that monitoring hospitalized cases may have been crucial at the pandemic's outset.

By comparing various models, we determined that incorporating an exposed class was essential. Neglecting this class would result in an immediate drop in infection numbers, which is not realistic given the latent period of the disease. Our models also included divisions between undetected/detected cases and asymptomatic/symptomatic courses, as these distinctions were necessary. Undetected cases have a higher transmission rate, and a significant proportion of individuals become infected by presymptomatic individuals. We also tried a model with a quarantine state for detected cases, but it did not improve the results (Supplemental Figure A1 bottom,

Supplemental Table A1). While other authors have previously used simpler models [13, 15, 16], our focus was on understanding the biological processes and parameters. Our data cover the first four pandemic's waves, and, therefore, some compartments of our model may not have been necessary for other analyses that concentrate on the reproduction number.

In the first half of 2021, new virus variants of SARS-CoV-2 were observed. When modeling the third wave, the much more contagious Alpha variant resulted in a higher transmission rate, being the cause of the outbreak of the third wave despite a lockdown being in place. In addition, when simulating the third wave, classes representing the vaccinated population had to be included into the model. Without taking into account the progressive immunization of the population at the end of the third wave, the number of cases in the model would increase again, although the data from the RKI show that the number of cases continue to decrease.

Predictions for different scenarios during the fourth wave are summarized in Figure 6. Even though a large proportion of the population is already vaccinated, the number of new COVID-19 cases is predicted to increase with rising contact rates and decreasing willingness to vaccinate. Rapid reopening with a standstill in vaccination could result in an extreme fourth wave with a higher incidence than the previous three. Furthermore, it was assumed that completely vaccinated individuals could no longer become infected with SARS-CoV-2. However, since it has been demonstrated that even completely vaccinated individuals can become infected, especially with the Delta variant, the daily incidence could be even higher than predicted by Model 2.8 [45].

Although the incidence during the fourth wave in the extreme scenario was even greater than during the second wave, we see in Figure 1(B) that the hospitalization rate decreases with an increasing number of fully vaccinated individuals. This confirms that vaccinations help against a severe course of COVID-19. However, the number of patients in normal wards could be higher than predicted since vaccine protection against a severe course wanes after approximately six months.

A discrepancy between IVENA data and model output was observed in Figure 5, where the number of hospitalized patients briefly decreased in the former while continuing to increase in the latter. This may be due to younger individuals being infected, and the lower hospitalization rate among them was not accounted for in the model. Barbarossa et al. [19] applied complex and age-structured SEIR models to incidence data, but they were without hospitalization information. Our models presented here could also be expanded with age structure. Differences in infections would be expected not only between age categories, but also between the pandemic waves.

The ICU occupancy could increase sharply even though the hospitalization rate decreased during the fourth wave due to the increasing immunity of the population. This is because non-vaccinated individuals are hospitalized and a large proportion of inpatients must be admitted to the ICU, which can still lead to an overload of the healthcare system.

In Figure 1(D), the hospitalization rate decreased during the fourth wave due to the increasing immunity of the population, but the number of ICU patients could again increase sharply. This is because non-vaccinated individuals are hospitalized [46] and a large proportion of inpatients must be admitted to the ICU, which can still lead to an overload of the healthcare system.

To summarize, we applied biology-based mathematical models to predict the fourth wave of COVID-19 in Munich. We give a rough idea of the possible courses of the pandemic and not an accurate prediction of a particular outcome. The best, most likely and worst case scenarios are presented to help policymakers make decisions about interventions. During the epidemic,

non-pharmaceutical interventions changed rapidly. Also, the introduction of vaccines and the advent of new variants significantly modified the settings of the pandemic. The models need to be adapted after every change, but since its structure remains similar and the computational time is short, this can be done quickly. The models applied are complex; therefore, the reliability of the parameters was supported by splitting the analysis in two steps: the incidence data supporting the biology-pandemic-dependent parameters, while the hospital data were used to support the hospitalization process. We have to underline that the forecasts presented here completely depend on the previously fitted parameters. The next steps could be to add a sensitivity analysis to show dependencies.

During the first three waves, the incidence and the 7-day incidence were key indicators for interventions, but since a large part of the population in Munich is fully vaccinated, the importance of incidences as an indicative value decreases while that of the hospitalization rate and ICU treatments increases. The incidence must still be monitored in the future since the higher the incidence, the more difficult it will be to track contacts and use interventions to keep infection numbers down. We support the thesis that monitoring the hospitalization should have been introduced at the beginning of the pandemic, together with the 7-day incidence, to clarify its importance and avoid miscommunication with the members of the public.

Acknowledgments

This work was supported by the Bavarian State Ministry of Science and the Arts; University Hospital; Ludwig Maximilian University Munich; German Ministry for Education and Research (proj. nr.: 01KI20271).

Conflict of interest

The authors declare that there is no conflict of interest.

Code availability

To facilitate reproducibility and reuse, we made the code used to perform the analyses and generate the figures available on GitHub (accessed on November 30, 2022) https://github.com/NoemiCastelletti/Hospitalization_Munich_COVID-19.git.

References

1. B. Ganesh, T. Rajakumar, M. Malathi, N. Manikandan, J. Nagaraj, A. Santhakumar, et al., Epidemiology and pathobiology of SARS-CoV-2 (COVID-19) in comparison with SARS, MERS: An updated overview of current knowledge and future perspectives, *Clin. Epidemiol. Glob. Health*, **10** (2021), 100694. https://doi.org/10.1016/j.cegh.2020.100694
2. World Health Organization, WHO Director-General's Opening Remarks at the Media Briefing on COVID-19-11 March 2020, 2020. Available from: https://www.who.int/director-general/speeches/detail/who-director-general-s-opening-remarks-at-the-media-briefing-on-covid-19---11-march-2020

3. World Health Organization, WHO Coronavirus (COVID-19) Dashboard, 2022. Available from: https://covid19.who.int/
4. Robert Koch-Institute (RKI), Table showing current Covid-19 infections per day as time series, 2021. Available from: https://npgeo-corona-npgeo-de.hub.arcgis.com/datasets/dd4580c810204019a7b8eb3e0b329dd6_0/explore
5. Robert Koch-Institute (RKI), Kontaktpersonen-Nachverfolgung bei SARS-CoV-2-Infektionen, 2021. Available from: https://www.rki.de/DE/Content/InfAZ/N/Neuartiges_Coronavirus/Kontaktperson/Management.html;jsessionid=78E4E999E14B2E6A3E8F02E5957D2C97.internet121?nn=13490888#doc13516162bodyText14
6. Robert Koch-Institute (RKI), Tabelle mit den gemeldeten Impfungen nach Bundesländern und Impfquoten nach Altersgruppen, 2021. Available from: https://www.rki.de/DE/Content/InfAZ/N/Neuartiges_Coronavirus/Daten/Impfquotenmonitoring
7. Robert Koch-Institute (RKI), Kurz und Knapp: Faktenblätter zum Impfen - COVID-19 Impfung, 2021. Available from: https://www.rki.de/DE/Content/Infekt/Impfen/Materialien/Faktenblaetter/Faktenblaetter_inhalt.html
8. J. Schilling, A. Lehfeld, D. Schumacher, M. Diercke, S. Buda, W. Haas, et al., Krankheitsschwere der ersten COVID-19-Welle in Deutschland basierend auf den Meldungen gemäß Infektionsschutzgesetz, *J. Health Monit.*, **5** (2020), 2–20. https://doi.org/10.25646/7169
9. Centers for Disease Control and Prevention (CDC), National Center for Immunization and Respiratory Diseases (NCIRD), Disease Burden of Flu, 2022. Available from: https://www.cdc.gov/flu/about/burden/index.html/
10. Robert Koch-Institute (RKI), Coronavirus SARS-CoV-2: Fallzahlen und Meldungen, 2021. Available from: https://www.rki.de/SharedDocs/FAQ/NCOV2019/FAQ_Liste_Fallzahlen_Meldungen.html
11. R. M. Anderson, The role of mathematical models in the study of HIV transmission and the epidemiology of AIDS, *J. Acquir. Immune Defic. Syndr.*, **1** (1988), 241–256.
12. F. Brauer, C. Castillo-Chavez, *Mathematical Models in Population Biology and Epidemiology*, Springer, New York, 2012.
13. D. Chumachenko, I. Meniailov, K. Bazilevych, T. Chumachenko, S. Yakovlev, Investigation of statistical machine learning models for COVID-19 epidemic process simulation: Random Forest, K-Nearest Neighbors, Gradient Boosting, *Computation*, **10** (2022), 2079–3197. https://doi.org/10.3390/computation10060086
14. F. Ying, N. O'Clery, Modelling COVID-19 transmission in supermarkets using an agent-based model, *PLoS One*, **16** (2021), 0249821. https://doi.org/10.1371/journal.pone.0249821

15. R. Nistal, M. de la Sen, J. Gabirondo, S. Alonso-Quesada, A. J. Garrido, I. Garrido, A Study on COVID-19 incidence in Europe through two SEIR epidemic models which consider mixed contagions from asymptomatic and symptomatic individuals, *Appl. Sci.*, **11** (2021), 2076–3417. https://doi.org/10.3390/app11146266

16. R. Nistal, M. de la Sen, J. Gabirondo, S. Alonso-Quesada, A. J. Garrido, I. Garrido, A Modelization of the Propagation of COVID-19 in regions of Spain and Italy with evaluation of the transmission rates related to the intervention measures, *Biology*, **10** (2021), 121. https://doi.org/10.3390/biology10020121

17. J. Ozaki, Y. Shida, H. Takayasu, M. Takayasu, Direct modelling from GPS data reveals daily-activity-dependency of effective reproduction number in COVID-19 pandemic, *Sci Rep.*, **12**, (2022), 17888. https://doi.org/10.1038/s41598-022-22420-9

18. D. Okuonghae, A. Omame, Analysis of a mathematical model for COVID-19 population dynamics in Lagos, Nigeria, *Chaos, Solitons Fractals*, **139** (2020), 110032. https://doi.org/10.1016/j.chaos.2020.110032

19. M. V. Barbarossa, J. Fuhrmann, J. H. Meinke, S. Krieg, H. V. Varma, N. Castelletti, et al., Modeling the spread of COVID-19 in Germany: Early assessment and possible scenarios, *PLoS ONE*, **15**, (2020). https://doi.org/10.1371/journal.pone.0238559

20. Süddeutsche Zeitung, Coronavirus-Pandemie in Bayern: Rückblick April 2020, *Süddeutsche Zeitung*, 2020. Available from: https://www.sueddeutsche.de/bayern/coronavirus-bayern-rueckblick-april-1.4873340

21. Norddeutscher Rundfunk, Corona-Chronologie: November 2020, 2020. Available from: https://www.ndr.de/nachrichten/info/Corona-Chronologie-November-2020,coronachronologie128.html

22. Norddeutscher Rundfunk, Corona-Chronologie: Dezember 2020. Available from: https://www.ndr.de/nachrichten/info/Corona-Chronologie-Dezember-2020,coronachronologie130.html

23. Norddeutscher Rundfunk, Corona-Chronologie: Januar 2021, 2021. Available from: https://www.ndr.de/nachrichten/info/Corona-Chronologie-Januar-2021,coronachronologie134.html

24. Süddeutsche Zeitung, Was in München ab heute gilt, 2021. Available from: https://www.sueddeutsche.de/muenchen/muenchen-corona-notbremse-mittwoch-1.5263849

25. Süddeutsche Zeitung,Diese Corona-Regeln gelten nun in München, 2021. Available from: https://www.sueddeutsche.de/muenchen/muenchen-corona-lockerungen-gastronomie-ausgangssperre-1.5288681

26. Bayerische Staatsregierung, Pressemitteilungen: Bericht aus der Kabinettssitzung vom 4. Juni 2021, 2021. Available from: https://www.bayern.de/bericht-aus-der-kabinettssitzung-vom-4-juni-2021/

27. Deutsche Akademie der Naturforscher Leopoldina, Ad-hoc-Stellungnahmen zur Coronavirus-Pandemie: Zusammenfassung der Stellungnahmen zur Coronavirus-Pandemie, 2020.

28. H. Panknin, S. Schröder, Konsequente Schutzmaßnahmen gegen Ansteckung, *Procare*, **25**, (2020), 20–22. https://doi.org/10.1007/s00735-020-1261-x

29. Robert Koch-Institute (RKI), Übersicht zu besorgniserregenden SARS-CoV-2-Virusvarianten (VOC), 2021. Available from: https://www.rki.de/DE/Content/InfAZ/N/Neuartiges_Coronavirus/Virusvariante.html

30. Robert Koch-Institute (RKI), Berichte zu Virusvarianten von SARS-CoV-2 in Deutschland, 2021. Available from: https://www.rki.de/DE/Content/InfAZ/N/Neuartiges_Coronavirus/DESH/Berichte-VOC-tab.html

31. Robert Koch-Institute (RKI), SARS-CoV-2: Virologische Basisdaten sowie Virusvarianten, 2021. Available from: https://www.rki.de/DE/Content/InfAZ/N/Neuartiges_Coronavirus/Virologische_Basisdaten.html;jsessionid=A1752CE0733B8B43969A64CD80B9B253.internet082?nn=13490888

32. Landeshauptstadt München-Das offizielle Stadtportal, Coronavirus-Fälle in München: Aktuelle Zahlen, 2021. Available from: https://www.muenchen.de/rathaus/Stadtinfos/Coronavirus-Fallzahlen.html

33. E. Callaway, Delta coronavirus variant: scientists brace for impact, *Nature*, (2021), 17–18. https://doi.org/10.1038/d41586-021-01696-3

34. BR24, Corona-Regeln: Was aktuell in Bayern gilt, 2021. Available from: https://www.br.de/nachrichten/bayern/corona-regeln-in-bayern-was-gilt,Sbtbuu0

35. Süddeutsche Zeitung, Corona in Bayern: Newsblog vom 5. bis zum 26. Juli 2021, 2021. Available from: https://www.sueddeutsche.de/bayern/corona-bayern-archiv-1.5342370

36. Süddeutsche Zeitung, Corona-Regeln Bayern: Welche Regeln aktuell in Bayern gelten, 2021. Available from: https://www.sueddeutsche.de/bayern/bayern-corona-regeln-2g-3g-maskenpflicht-1.4878824

37. C. Walter, F. Fischer, Interdisciplinary Supply Proof (IVENA): Improving Emergency Care through E-Health?, *NOTARZT*, **33**, (2017), 50.

38. Robert Koch-Institute (RKI), Epidemiologischer Steckbrief zu SARS-CoV-2 und COVID-19, 2021. Available from: https://www.rki.de/DE/Content/InfAZ/N/Neuartiges_Coronavirus/Steckbrief.html;jsessionid=1E68F40DA18BE45CC49EE51EA8FA8CC8.internet051?nn=2386228

39. S. Amit, G. Regev-Yochay, A. Afek, Y. Kreiss, E. Leshem, Early rate reductions of SARS-CoV-2 infection and COVID-19 in BNT162b2 vaccine recipients, *Lancet*, **397**, (2021), 875–877. https://doi.org/10.1016/s0140-6736(21)00448-7

40. H. Xin, Y. Li, P. Wu, Z. Li, E. H. Y. Lau, Y. Qin, et al., Estimating the latent period of coronavirus disease 2019 (COVID-19), *Clin. Infect. Dis.*, **74** (2022), 1678–1681. https://doi.org/10.1093/cid/ciab746

41. D. Buitrago-Garcia, D. Egli-Gany, M. J. Counotte, S. Hossmann, H. Imeri, A. M. Ipekci, et al., Occurrence and transmission potential of asymptomatic and presymptomatic SARS-CoV-2 infections: A living systematic review and meta-analysis, *PLoS Med.*, **17**, (2020). https://doi.org/10.1371/journal.pmed.1003346

42. Bayerisches Landesamt für Statistik, Die Datenbank des Bayerischen Landesamtes für Statistik, 2023. Available from: https://www.statistikdaten.bayern.de/genesis/online;jsessionid%3D6CB3363574391F9435FD661D9125B699?sequenz%3DtabelleErgebnis%26selectionname%3D12411-001

43. N. Potere, E. Valeriani, M. Candeloro, M. Tana, E. Porreca, A. Abbate, et al., Acute complications and mortality in hospitalized patients with coronavirus disease 2019: A systematic review and meta-analysis, *Crit. Care*, **24** (2020), 1–12. https://doi.org/10.1186/s13054-020-03022-1

44. M. Martcheva, *An Introduction to Mathematical Epidemiology*, Springer, New York, 2015.

45. Y. Goldberg, M. Mandel, Y. M. Bar-On, O. Bodenheimer, L. S. Freedman, E. Haas, et al., Waning immunity of the BNT162b2 vaccine: A nationwide study from Israel, *New Engl. J. Med.*, (2021). https://doi.org/10.1056/nejmoa2114228

46. BR24, Covid-19 in den Kliniken: Die Welle der Ungeimpften, 2021. Available from: https://www.br.de/nachrichten/bayern/covid-19-in-den-kliniken-die-welle-der-ungeimpften,SjYWL3B

47. K. P. Burnham, D. R. Anderson, *Model Selection and Multimodel Inference*, Springer, New York, 2002.

48. M. L. Gavrilova, O. Gervasi, V. Kumar, C. J. K. Tan, D. Taniar, A. Laganà, et al., Computational science and its applications-ICCSA 2006: international conference, Glasgow, in *ICCSA: International Conference on Computational Science and Its Applications*, **3982** (2006).

Supplementary

Model selection

Model selection is the task of choosing the best model out of a set of candidate models with the smallest possible number of parameters, which still represents the data adequately [47]. A model with too few parameters can lead to underfitting, not capturing the true relationship in the data. In contrast, a model with too many parameters can lead to overfitting, capturing the noise in the underlying data [47]. Assume a set of data $D : (x_i, y_i)$ is generated by a true function $y = f(x) + \epsilon$, where ϵ is the noise of the data (normally distributed with mean $E[\epsilon] = 0$ and variance $Var[\epsilon] = \sigma^2$). The unknown function $\hat{f}(x)$ can be fitted to the data minimizing the SSE, and the formula for the expected error has the form [48]

$$E[(y^* - \hat{f}(x^*))^2] = \sigma^2 + Bias^2(\hat{f}(x^*)) + Variance(\hat{f}(x^*)). \tag{A.1}$$

From (A.1) we can see that the expected error between the data points and the model depends on the noise, the bias and the variance. The noise is difficult to reduce because, in practice, it is often unknown. Bias and variance depend instead on the complexity of the model. If model complexity (i.e., the number of parameters) increases, the bias decreases, whereas the variance increases. On the other hand, if model complexity decreases, the bias increases while the variance decreases [48]. The goal is to minimize the expected error between the model and the data, which is equivalent to minimizing the bias and the variance of the model. It follows that both a too simple model and a too complex model are not optimal, as the data will either be underfitted or overfitted.

In this analysis, model selection was performed by applying the AIC, which measures the relative goodness of fit of a mathematical model [44]. For a given model, the AIC is computed as

$$AIC = n[\ln(\frac{SSE}{n})] + 2(k+1), \tag{A.2}$$

where n is the number of available data points in the dataset, k is the number of unknown parameters to be fitted, and SSE is the least-squares error [44].

We calculate the AIC for each candidate model. The best model is the one with the smallest AIC. From (A.2), we can see that the AIC is directly proportional to the number of fitted parameters, penalizing too complex models and, hence, preventing overfitting [44]. In addition, the AIC rewards models with a good fit, i.e., models with a small SSE, which prevents underfitting.

Table A1. Comparison of model attempts

Model	SSE	No. Parameters	AIC
Model 1	659041.0	1	937.6512
Model 2	231249.3	1	825.5912
Preferred model	108642.9	3	748.7602
Model 3	114436.7	3	754.3195

Defining the preferred model

Now, the question is, which models can capture the data best while also not being unnecessarily complicated? For this purpose, the AIC values of the four different models are compared in Table A1. We can see that the preferred model has the smallest AIC value. Therefore, the preferred model is the most appropriate among all four candidate models for simulating the first wave of COVID-19 in Munich. By comparing the AIC from Model 1 and Model 2, it follows that the inclusion of an exposed class is essential, as the AIC decreases significantly. Additionally, a significant improvement in AIC follows from the differentiation between undetected and detected cases, as well as between individuals with asymptomatic and symptomatic course. This suggests that undetected infectious individuals and individuals without any symptoms also play an important role in the dynamics of the pandemic. For instance, according to the RKI, a relevant proportion of people become infected via presymptomatic individuals [38]. The inclusion of a quarantine compartment does not improve the AIC, at least under the current conditions, which suggests that Model 3 is unnecessarily complicated. Since the preferred model can best simulate the first wave of the COVID-19 pandemic in Munich, it is also the model used for the analysis of the other pandemic waves.

Model Attempts

Model 1: SIR Model

First, we attempted to model the first wave of COVID-19 by using the basic SIR model (Figure A1(A)) [12]. It was assumed that the susceptible individuals (S) have not yet had the disease but can become infected through contact with an infected individual (I). Furthermore, for this model, only detected cases are considered to make it possible to compare model output and the RKI data. Approximately 10 days after symptom onset, the contagiousness of the infected person decreases

significantly [38]. After recovery of infected individuals (R), they become immune to reinfection. Further details on parameter assumptions are given in Table A2. Model 1 is then given by the following system of differential equations:

$$\begin{aligned} \dot{S} &= -\lambda S, \\ \dot{I} &= \lambda S - \alpha I, \\ \dot{R} &= \alpha I, \end{aligned}$$

where $\lambda(t) = \beta(t)\frac{I(t)}{N}$ is the force of infection and $N \approx 1.484$ million is the total population size of Munich [42]. Furthermore, $\beta(t)$ is the time-dependent transmission rate. Since the RKI reported one COVID-19 case on the first day of the first wave, we used $S(0) = N - 1$, $I(0) = 1$ and $R(0) = 0$ as initial values for the three compartments.

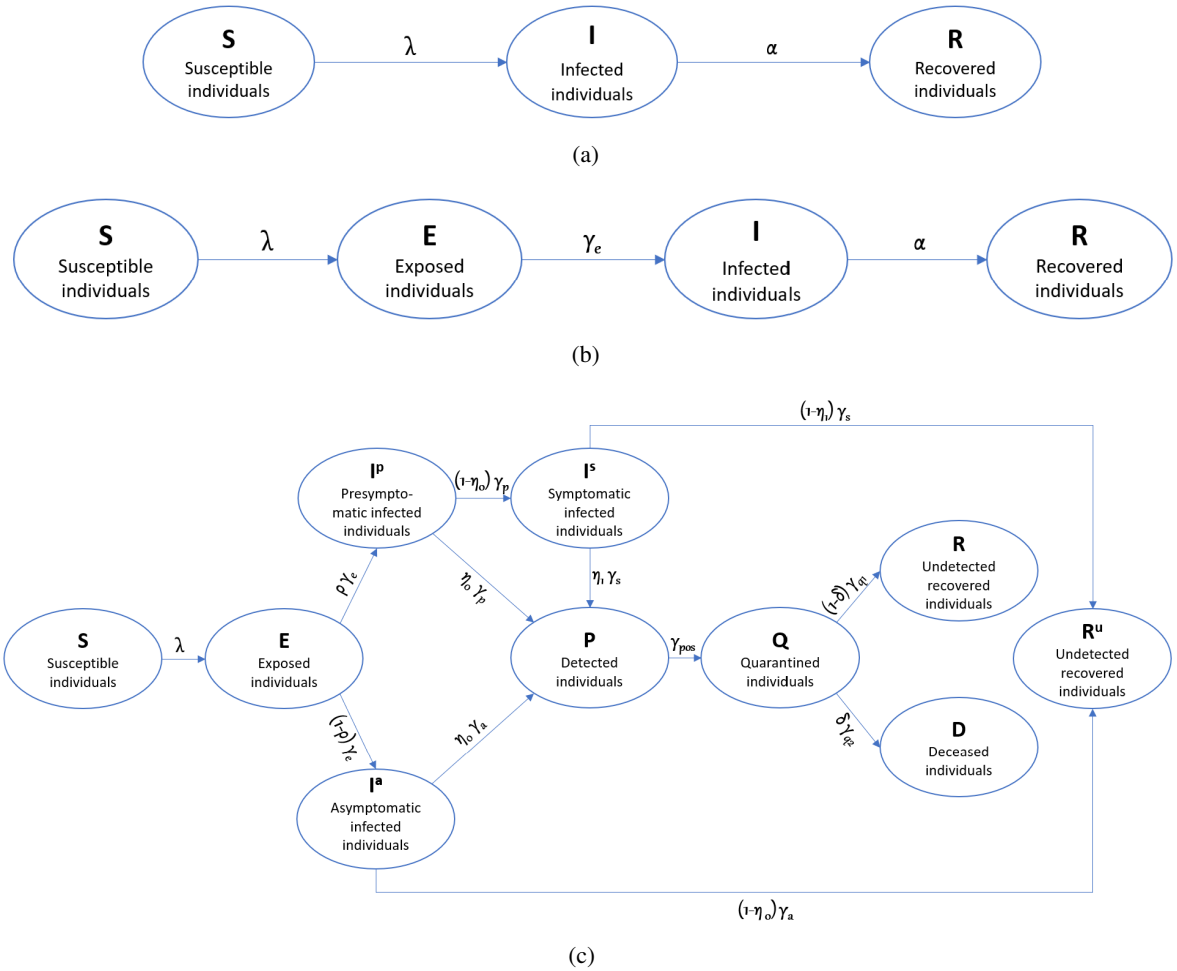

Figure A1. Scheme of the model attempts: (A) Model 1, (B) Model 2 and (C) Model 3.

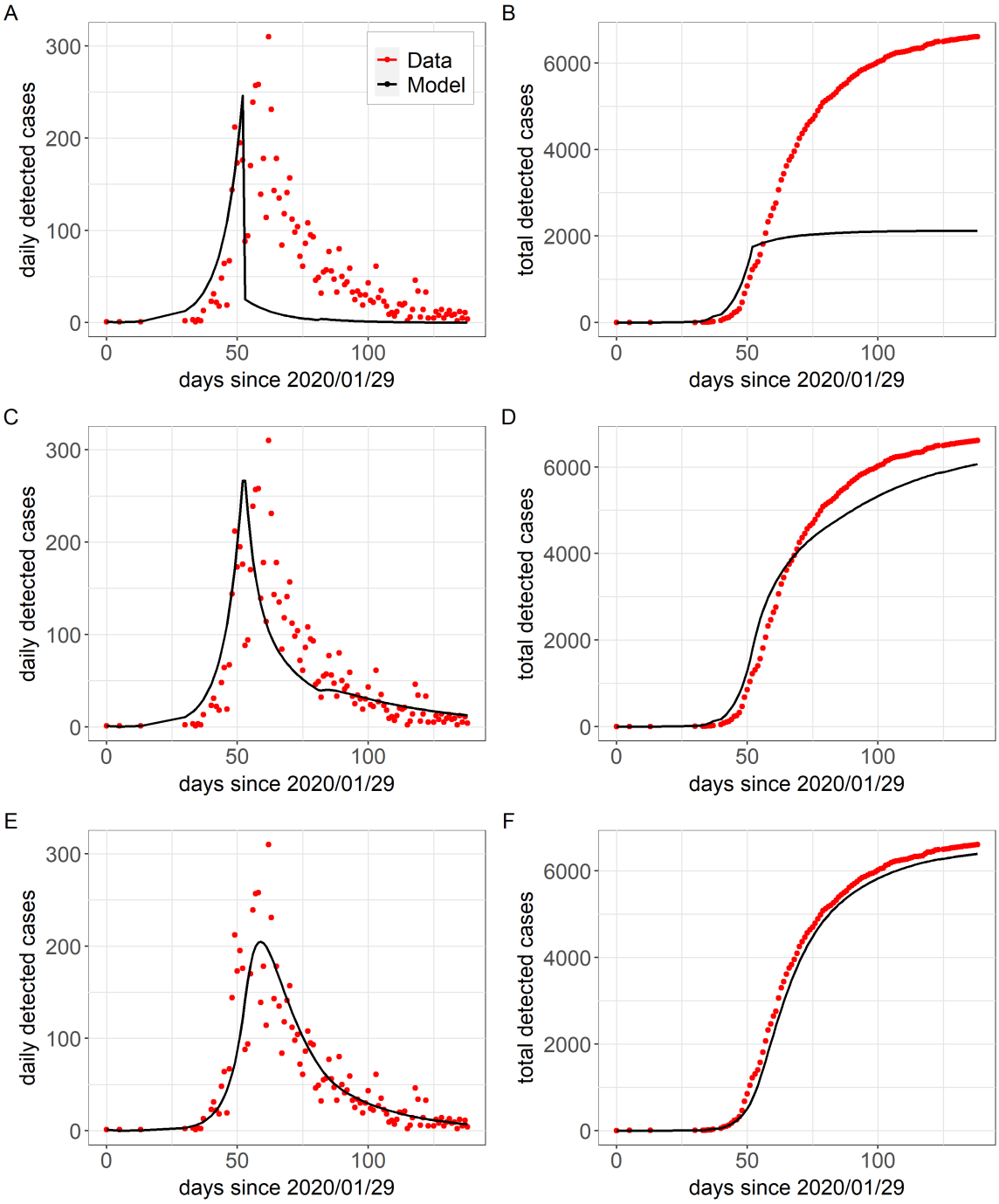

Figure A2. Performance evaluation of the model attempts. Comparison of model output (black) with RKI data (red). (A), (C) and (D): Daily detected COVID-19 cases in Munich in wave one for Models 1, 2 and 3, respectively. (B), (D) and (E): Total detected COVID-19 cases in Munich in wave one for Models 1, 2 and 3, respectively. The basic SIR Model 1 cannot capture the structure of the data. The SEIR Model 2 shows a clear improvement compared to the SIR model. The more complex Model 3 can capture the structure of the data very well, with, however, a worse AIC than the preferred model.

To compare Model 1 with the RKI data, we calculate the newly detected infections $\hat{d}(t)$ at day t from the output of Model 1 as follows:

$$\hat{d}(t) = \begin{cases} I(0) & \text{if } t = 0 \\ S(t) - S(t+1) & \text{if } t > 0. \end{cases}$$

In Figure A2(A) and (b), it can be seen that the simple SIR model cannot capture the spread of COVID-19 in Munich during the first wave. One reason for this is the exclusion of an exposed class. When the lockdown starts after 52 days and the transmission rate decreases, we can see that the number of infected individuals immediately drop off. However, this is not realistic because, at this point in time, there are a lot of individuals who are already infected with COVID-19 but neither have symptoms nor are they infectious. These individuals are called exposed individuals. After infection with the disease, the virus needs some time to develop in the human body. The time during which an individual is infected but not yet infectious is called the latent period [44]. So, at the start of the lockdown, there are still a lot of individuals moving to the infected class although there are no or less new infections. So, for the next model, we will include an exposed (latent) class.

Model 2: Including an Exposed Class

In addition to the three compartments of the previous model, an exposed class (E) is now included in Model 2 (Figure A1 middle). After infection, individuals move from the susceptible to the exposed class, where they have neither symptoms nor are they infectious. After a latent period of approximately 5.5 days, the infected individuals become infectious and develop symptoms and therefore move to class I [38]. Details on parameter assumptions are given in Table A2.
Model 2 is then given by the following system of differential equations:

$$\begin{aligned} \dot{S} &= -\lambda S, \\ \dot{E} &= \lambda S - \gamma_e E, \\ \dot{I} &= \gamma_e E - \alpha I, \\ \dot{R} &= \alpha I, \end{aligned}$$

where, again, $\lambda(t) = \beta(t)\frac{I(t)}{N}$ is the force of infection and $\beta(t)$ the time-dependent transmission rate. As initial values for the four compartments, $S(0) = N - 1$, $E(0) = 0$, $I(0) = 1$ and $R(0) = 0$ were used.

The newly infected individuals $\hat{d}(t)$ at day t are calculated from the output of the SEIR model as follows:

$$\hat{d}(t) = \begin{cases} I(0) & \text{if } t = 0, \\ [I(t+1) - I(t)] + [R(t+1) - R(t) & \text{if } t > 0. \end{cases}$$

After minimizing the SSE between the daily detected COVID-19 cases $d(t)$ reported by the RKI and $\hat{d}(t)$ from the model output, the results of the fitted model can be seen in Figure A2(c)–(d). Compared to Model 1, a significant improvement in the performance of Model 2 can be recognized.

Table A2. Parameters of Models 1, 2 and 3 for the first wave

Parameter	Description	Value (unit) [Refs.]
Model 1		
β_0	Initial transmission rate	0.24 $\frac{1}{d\cdot\text{individual}}$ [fitted]
$\frac{1}{\alpha}$	Mean duration of infection	10 d [38]
Model 2 (added parameters)		
β_0	Initial transmission rate	0.45 $\frac{1}{d\cdot\text{individual}}$ [fitted]
$\frac{1}{\gamma_e}$	Mean duration of latent phase	5.5 d [38]
Model 3 (added parameters)		
β_0	Initial transmission rate	0.67 $\frac{1}{d\cdot\text{individual}}$ [fitted]
η_0	Prob. of detection while asympt.	0.62 [fitted]
$\frac{1}{\gamma_{pos}}$	Mean duration to go to quarantine	1 d [assumed]
$\frac{1}{\gamma_{q_1}}$	Mean duration of quarantine	14 d [5]
$\frac{1}{\gamma_{q_2}}$	Mean duration from start of quarantine until death	2 d [fitted]

Model 3: Including Quarantine

We extended the model presented in the main manuscript (called the preferred model in the following) and have included a compartment representing the quarantined individuals (Q) (Figure A1 bottom). All people with a detected SARS-CoV-2 infection go directly into quarantine, where they are supposed to have no contact with other people. Therefore, we assume that individuals who are in compartment Q can no longer infect anyone. During quarantine, individuals can die because of the disease and then move to the deceased compartment D, or they leave quarantine after approximately 14 days and go to the recovered compartment R [5].

Model 3 is then given by the following system of differential equations:

$$
\begin{aligned}
\dot{S} &= -\lambda S, \\
\dot{E} &= \lambda S - \gamma_e E, \\
\dot{I}^a &= (1-\rho)\gamma_e E - \gamma_a I_a, \\
\dot{I}^p &= \rho\gamma_e E - \gamma_p I_p, \\
\dot{I}^s &= (1-\eta_0)\gamma_p I_p - \gamma_s I_s, \\
\dot{P} &= \eta_0\gamma_a I_a + \eta_0\gamma_p I_p + \eta_1\gamma_s I_s - \gamma_{pos} P, \\
\dot{Q} &= \gamma_{pos} P - (1-\delta)\gamma_{q_1} Q - \delta\gamma_{q_2} Q, \\
\dot{R} &= (1-\delta)\gamma_{q_1} Q, \\
\dot{D} &= \delta\gamma_{q_2} Q, \\
\dot{R}^u &= (1-\eta_1)\gamma_s I_s + (1-\eta_0)\gamma_a I_a,
\end{aligned}
$$

where the force of infection $\lambda(t)$ is time-dependent and defined like before in the model presented in the main manuscript. In addition to the initial values from the main model, we used $Q(0) = 0$. The

parameters can be found in Table A2.

It follows that the number of daily detected infections in Model 3 is described by the class P, i.e., $\hat{d}(t) = P(t)$. After minimizing the SSE between the daily detected COVID-19 cases $d(t)$ reported by the RKI and $\hat{d}(t)$, the results of the fitted model can be seen in Figure A2(e)–(f). The performance of Model 3 seems very similar to that of the preferred model, however, without any improvement in the goodness of fit (Table A1).

Model analysis

As part of a standard analysis for such epidemiological models, one may be interested in the reproduction number R. To establish a unique disease-free equilibrium, we modify the model in such a way that we take into account the (slow) population dynamics. For that, we assume that all newborns (constant rate Λ) go into the susceptible compartment, and we have a natural per capita death rate μ for all compartments. The compartment D is left out for that purpose. The model version for this analysis reads as

$$\begin{aligned}
\dot{S} &= \Lambda - \lambda(t)S - v_1 S - \mu S,\\
\dot{E} &= \lambda(t)S + \sigma\lambda V_1 - \gamma_e E - \mu E,\\
\dot{V}_1 &= v_1 S - \sigma\lambda V_1 - v_2 V_1 - \mu V_1,\\
\dot{V}_2 &= v_2 V_1 - \mu V_2,\\
\dot{I}^a &= (1-\rho)\gamma_e E - \gamma_a I^a - \mu I^a,\\
\dot{I}^p &= \rho\gamma_e E - \gamma_p I^p - \mu I^p,\\
\dot{I}^s &= (1-\eta_0)\gamma_p I^p - \gamma_s I^s - \mu I^s,\\
\dot{P} &= \eta_0\gamma_a I^a + \eta_0\gamma_p I^p + \eta_1\gamma_s I^s - (h_0\gamma_{pos_1} + (1-h_0)\gamma_{pos_2})P - \mu P,\\
\dot{H}^{norm} &= h_0\gamma_{pos_1}P + (1-\delta)\gamma_{icu}H^{ICU} - (h_1\gamma_{norm_1} + (1-h_1)\gamma_{norm_2})H^{norm} - \mu H^{norm},\\
\dot{H}^{ICU} &= h_1\gamma_{norm_1}H^{norm} - \gamma_{icu}H^{ICU} - \mu H^{ICU},\\
\dot{R} &= (1-\eta_0)\gamma_a I^a + (1-\eta_1)\gamma_s I^s + (1-h_0)\gamma_{pos_2}P + (1-h_1)\gamma_{norm_2}H^{norm} - \mu R,
\end{aligned} \tag{A.3}$$

still with $\lambda(t) = \frac{\beta_a I^a + \beta_p I^p + \beta_s I^s + \beta_{pos} P}{N-D}$ and N the total population size. In this model version, as well as in the versions in the main part, the non-negativity of solutions is kept when starting with non-negative initial values. This can be easily seen because all negative terms on the right-hand side are proportional to the respective variable. Furthermore, by having a compartmental model including a constant birth term and death terms in all compartments, the solutions stay bounded. Here, we use a constant $\beta_a(t)$. Setting the right-hand sides of (A.3) equal to zero, we can easily solve it for the disease-free equilibrium, which reads as

$$(\hat{S}, 0, \hat{V}_1, \hat{V}_2, 0, 0, 0, 0, 0, 0, 0) = (\Lambda/(v_1+\mu), 0, \frac{v_1}{(v_2+\mu)(v_1+\mu)}\Lambda, \frac{v_2 v_1}{\mu(v_2+\mu)(v_1+\mu)}\Lambda, 0, 0, 0, 0, 0, 0, 0).$$

The total population in this equilibrium situation is $N = \Lambda \cdot \frac{(v_2+\mu)\mu + v_1\mu}{(v_1+\mu)(v_2+\mu)\mu}$.

Please note that, for the disease-free equilibrium, it does not matter that $\lambda(t)$ is not constant, as this term becomes equal to zero; also, it is an autonomous equation, which means that, even if we calculate an endemic equilibrium, it would work.

We follow the van den Driessche and Watmough approach for calculating the reproduction number as formulated in [44]. For that, we need to sort the compartments into infected ones, $X = (E, I^a, I^p, I^s, P)$, and the non-infected ones, $Y = (S, V_1, V_2, R)$ (the hospital compartments are left out for this purpose, as they do not have any further influence). Next, we split the right-hand side terms of X into new infections in the compartment and remaining terms, i.e.,

$$X' = F(X,Y) - V(x,Y) = \begin{pmatrix} \lambda(t)S + \sigma\lambda V_1 \\ (1+\rho)\gamma_e E \\ \rho\gamma_e E \\ (1-\eta_0)\gamma_p I_p \\ \eta_0\gamma_a I_a + \eta_0\gamma_p I_p + \eta_1\gamma_s I_s \end{pmatrix} - \begin{pmatrix} \gamma_e E \\ \gamma_a I_a \\ \gamma_p I_p \\ \gamma_s I_s \\ (h_0\gamma_{pos1} + (1-h_0)\gamma_{pos2})P \end{pmatrix};$$

F and V have to satisfy some general conditions, as $F_i(0,Y) = 0$ and $V_i(0,Y) = 0$ for $i = 1,\dots,5$, $F_i(X,Y) \geq 0$ for all $X, Y \geq 0$, $V_i(X,Y) \leq 0$ for $X_i = 0, i = 1,\dots,5$, and $\sum_{i=1}^{5} V_i(X,Y) \geq 0$ for all $X, Y \geq 0$, which is easy to see in this case. Next, we need two matrices (using the notation $Y_0 = (\hat{S}, \hat{V}_1, \hat{V}_2, 0)$):

$$\mathcal{F} = \left[\frac{\partial F_i(0,Y_0)}{\partial X_j}\right] = \begin{pmatrix} 0 & \frac{\beta_a\hat{S}}{N} + \frac{\sigma\beta_a\hat{V}_1}{N} & \frac{\beta_p\hat{S}}{N} + \frac{\sigma\beta_p\hat{V}_1}{N} & \frac{\beta_s\hat{S}}{N} + \frac{\sigma\beta_s\hat{V}_1}{N} & \frac{\beta_{pos}\hat{S}}{N} + \frac{\sigma\beta_{pos}\hat{V}_1}{N} \\ (1-\rho)\gamma_e & 0 & 0 & 0 & 0 \\ \rho\gamma_e & 0 & 0 & 0 & 0 \\ 0 & 0 & (1-\eta_0)\gamma_p & 0 & 0 \\ 0 & \eta_0\gamma_a & \eta_0\gamma_p & \eta_1\gamma_s & 0 \end{pmatrix}$$

and

$$\mathcal{V} = \left[\frac{\partial V_i(0,Y_0)}{\partial X_j}\right] = \begin{pmatrix} \gamma_e & 0 & 0 & 0 & 0 \\ 0 & \gamma_a & 0 & 0 & 0 \\ 0 & 0 & \gamma_p & 0 & 0 \\ 0 & 0 & 0 & \gamma_s & 0 \\ 0 & 0 & 0 & 0 & \underbrace{(h_0\gamma_{pos1} + (1-h_0)\gamma_{pos2})}_{=:h^*} \end{pmatrix}.$$

The latter one, being a diagonal matrix, can be easily inverted, which we need in the following step. For easier writing and to make the structure of the matrix more visible, we introduce the short notations $B_1 := \frac{\beta_a\hat{S}}{N\gamma_1} + \frac{\sigma\beta_a\hat{V}_1}{N\gamma_1}$, $B_2 := \frac{\beta_p\hat{S}}{N\gamma_p} + \frac{\sigma\beta_p\hat{V}_1}{N\gamma_p}$, $B_3 := \frac{\beta_s\hat{S}}{N\gamma_s} + \frac{\sigma\beta_s\hat{V}_1}{N\gamma_s}$ and $B_4 := \frac{\beta_{pos}\hat{S}}{Nh^*} + \frac{\sigma\beta_{pos}\hat{V}_1}{Nh^*}$. Then, we find that

$$K = \mathcal{F}\mathcal{V}^{-1} = \begin{pmatrix} 0 & B_1 & B_2 & B_3 & B_4 \\ (1-\rho) & 0 & 0 & 0 & 0 \\ \rho & 0 & 0 & 0 & 0 \\ 0 & 0 & (1-\eta_0) & 0 & 0 \\ 0 & \eta_0 & \eta_0 & \eta_1 & 0 \end{pmatrix}.$$

The corresponding characteristic polynomial has the form

$$0 = \lambda \cdot \{-\lambda^4 + (\rho-1)[-B_1\lambda^2 - \eta_0 B_4\lambda^2] + \rho[B_2\lambda^2 + B_4\eta_0\lambda + B_4(1-\eta_0)\eta_1]\}$$

(λ denotes here the eigenvalues, not to mix up with the $\lambda(t)$ from the model formulation).

The square root of the spectral radius of this matrix would yield us the reproduction number. Unfortunately, only one eigenvalue can be read out easily, and that is the 0. For the others, we maintain the roots of a polynomial of grade four, but this formula is not convenient, and is thus not useful in the general form. But, using concrete parameter values, one could apply these in matrix K and calculate the eigenvalues, and, consequently, numerically calculate the spectral radius. Please recall that $\beta_a(t)$ may vary, e.g., due to restrictions, and also influence the reproduction number.

The calculation and consideration of the endemic equilibrium is left out here, as the long-time behavior might not be so relevant for this purpose, as too many other properties and environmental conditions change with time.

AIMS Press